AD-A248 058

Final Technical Report

Growth, Nitrogen Vacancy Reduction and Solid Solution Formation in Cubic GaN Thin Films and the Subsequent Fabrication of Superlattice Structures Using AlN and InN

Robert F. Davis, Zlatko Sitar, Michael J. Paisley, Joe J. Sumakeris,
Laura Smith, K. Shaun Ailey-Trent, and Dong W. Kum
Materials Science and Engineering Department
North Carolina State University
Campus Box 7907
Raleigh, NC 27695-7907

February 1992

92 3 30 017

92-07996

Best Available Copy

REPORT DOCUMENTATION PAGE

Public reporting burden for this collection of information is estimated to average 1 hour per response, including the time for reviewing instructions, searching existing data sources, gathering and maintaining the data needed, and completing and reviewing the collection of information. Send comments regarding this burden estimate or any other aspect of this collection of information, including suggestions for reducing this burden, to Washington Headquarters Services, Directorate for Information Operations and Reports, 1215 Jefferson Davis Highway, Suite 1204, Arlington, VA 22202-4302, and to the Office of Management and Budget, Paperwork Reduction Project (0704-0188), Washington, DC 20503.

1. AGENCY USE ONLY (Leave blank)	2. REPORT DATE February 1992	3. REPORT TYPE AND DATES COVERED Final Technical 6/1/86–12/31/91

4. TITLE AND SUBTITLE Growth, Nitrogen Vacancy Reduction and Solid Solution Formation in Cubic GaN Thin Films and the Subsequent Fabrication of Superlattice Structures Using AlN and InN

5. FUNDING NUMBERS
RST:s400001src05
S.O.:1114SS

6. AUTHOR(S)

Robert F. Davis

7. PERFORMING ORGANIZATION NAME(S) AND ADDRESS(ES)

North Carolina State University
Hillsborough Street
Raleigh, NC 27695

8. PERFORMING ORGANIZATION REPORT NUMBER

N00014-86-K-0686 P5

9. SPONSORING/MONITORING AGENCY NAME(S) AND ADDRESS(ES)

Sponsoring: ONR, 800 N. Quincy, Arlington, VA 22217
Monitoring: Office of Naval Research Resider, N66005
The Ohio State University Research Center
1314 Kinnear Road
Columbus, OH 43212-1194

10. SPONSORING/MONITORING AGENCY REPORT NUMBER

11. SUPPLEMENTARY NOTES

12a. DISTRIBUTION/AVAILABILITY STATEMENT

Approved for Public Release; Distribution Unlimited

12b. DISTRIBUTION CODE

13. ABSTRACT (Maximum 200 words)

An atomic layer epitaxy deposition system configured for the growth of thin films of the III-V nitrides of Al, Ga and In has been designed, constructed and commissioned. The system allows the introduction of up to 16 gases without mixing. Self-terminating growth of crystalline GaN films has been achieved on single crystal wafers of (0001) α(6H)-SiC. Results of analyses via Auger spectroscopy, electron microscopy and electron diffraction are described. Deposition of AlN and GaN via gas-source MBE was also continued during this period. The principal emphasis concerned the initial stages of growth of both compounds on the substrates of (00001) α(6H)-SiC and (0001) sapphire, as determined using X-ray photoelectron spectroscopy. An initial layer of silicon nitride formed on the surface of SiC prior to the deposition of either nitride. The deposition of GaN on sapphire followed the Stranski-Krastanov mode of nucleation and growth, while on SiC, characteristics of three-dimensional growth were evident. By contrast, AlN grew initially in a layer-by-layer mode. Deposition of GaN on vicinal (100) β-SiC during UV irradiation resulted in the formation of a new 4H polytype of this material. Deposition of BN via gas-source MBE on Cu(110) resulted in nanocrystalline cBN, films grown on (111) Cu resulted in h BN (graphitic phase) Similar studies using Si(100) substrates also resulted in the occurrence of cBN. The occurrence of the cubic polytype was enhanced while that of h-BN was discouraged with the use of the UV light at 400–500°C.

14. SUBJECT TERMS
gallium nitride, aluminum nitride, boron nitride, atomic layer epitaxy, layered structures, transmission electron microscopy, photoluminescence, gas-source MBE, laser ablation, borazine

15. NUMBER OF PAGES
55

16. PRICE CODE

17. SECURITY CLASSIFICATION OF REPORT	18. SECURITY CLASSIFICATION OF THIS PAGE	19. SECURITY CLASSIFICATION OF ABSTRACT	20. LIMITATION OF ABSTRACT
UNCLAS	UNCLAS	UNCLAS	SAR

Table of Contents

I. INTRODUCTION

Continued development and commercialization of optoelectronic devices, including light-emitting diodes and semiconductor lasers produced from III-V gallium arsenide-based materials, has also generated interest in the much wider bandgap semiconductor mononitride materials containing boron, aluminum, gallium, and indium. The majority of the studies have been conducted on pure gallium nitride thin films having the wurtzite structure, and this emphasis continues to the present day. Recent research has resulted in the fabrication of p-n junctions in both wurtzite gallium nitride and cubic boron nitride, the deposition of cubic gallium nitride, as well as the fabrication of multilayer heterostructures and the formation of thin film solid solutions. Chemical vapor deposition (CVD) has usually been the technique of choice for thin film fabrication. However, more recently these materials have also been deposited by plasma-assisted CVD, reactive ionized-cluster beam deposition and reactive and ionized molecular beam epitaxy.

The overall program objectives in this contract have been (1) the development and employment of atomic layer epitaxy as a low temperature deposition method for GaN (2) the determination of the chemistry and morphology inherent in the nucleation and growth of GaN and AlN on the substrates of α(6H)-SiC (0001) and sapphire (Al₂O₃) (0001) via gas-source molecular beam epitaxy (GSMBE) and (3) the deposition of films of AlN, GaN and BN using GSMBE. The procedures, results, discussions of these results and conclusions of these studies are summarized in the following sections with reference to appropriate SDIO/ONR reports for details. Note that each major section is self-contained with its own figures, tables and references.

II. ATOMIC LAYER EPITAXY OF GALLIUM NITRIDE

A. Introduction

At the present time, MBE and MOCVD are the two contenders for the growth of the most sophisticated semiconducting structures. Both can produce extremely thin layers and a wide range of compound semiconductors and heterostructures. However, in both techniques all the reactant species arrive simultaneously to the substrate. As such, the growth of the subsequent monolayer of the material may be initiated before the growth of the previous one is completed. As a result, the growth process occurs on several levels of monolayers. This occurs in practically all materials deposition systems and is easily observed via RHEED oscillations. One observes the damping of the oscillation amplitude with the film thickness. As a result, the RHEED oscillations usually disappear after 10-20 monolayers of growth.

The ultimate technique, with the best control over the composition and the surface morphology, may be the deposition of a single layer of the atoms of one of the components at a time. The single most successful method for achieving this is by Atomic Layer Epitaxy

(ALE), a technique patented by Suntola and Atson in 1977 [1]. They used this method for the deposition of the polycrystalline ZnSe on glass substrates because of their concern regarding thickness uniformity over large areas.

Initially it was thought that ALE was applicable only for II-VI compounds. However, it has been shown that it also works also for other compounds and elements. A comprehensive review of the ALE research on II-VI compounds has been published by Goodman and Pessa [2]. Considerable attention has been lately devoted to the ALE of GaAs, and several research groups have demonstrated the feasibility of the technique for Ga-based III-V compounds [3,4].

Atomic Layer Epitaxy can be achieved with many existing deposition techniques, and is best thought of as a special mode of operation of the known techniques, rather than an entirely new deposition method. Since ALE consists of deposition cycles in which a single monolayer of individual species is deposited at a time, the final film thickness depends only on the number of cycles and the lattice parameter of the material. Thus ALE offers the ultimate control over the thickness and morphology of the layers, and has also the potential for the achievement of very good stoichiometry and the reduction of point defects. Since the reactants remain separated throughout the deposition, homogeneous nucleation of the desired phase within the gas stream is minimized.

B. Experimental Procedure

1. Description of the III-V Nitride ALE System

To accomplish ALE of the III-V nitrides, a vacuum system has been designed, fabricated and commissioned which allows ALE deposition within the framework of organometallic (OM) CVD parameters. The system is configured to process one-inch wafers. Ultimately, the apparatus may be adapted to handle samples up to two inches in diameter. The system consists of three chambers; a load lock, a cleaning chamber and a growth chamber. It is made of stainless steel parts with knife edge seals and is high vacuum capable. Process gasses are regulated by mass flow controllers and pumped by a rotary vane pump. The ultimate vacuum is achieved by diffusion pumps.

The load lock is a simple five way cross that can hold up to five samples. All samples are introduced to and removed from the system through this chamber; it can be evacuated to the millitorr level.

After passing through the load lock, the samples are cleaned in a subsequent chamber using a remote argon plasma with the downstream injection of hydrogen. The cleaning chamber is evacuated to high vacuum using a diffusion pump, while the process gases used for cleaning are handled by a rotary vane pump through an automatic throttle valve. To assure identical sample cleaning within a run, up to four samples can be cleaned at a time.

This chamber is capable of performing many variations on the plasma cleaning operation, since it has the capability of varying gas flow rates, substrate temperature, plasma intensity and process pressure.

After cleaning, the samples are transferred to the growth chamber. This chamber is also evacuated to high vacuum using a diffusion pump with an LN_2 trap, while the process gases are handled by a rotary vane pump. The volatile exhaust gases in the growth and cleaning chambers are diluted with nitrogen and cleaned in a water scrubber prior to the release into central exhaust system. The process pressure is monitored and controlled by a capacitance pressure gauge and an automatic throttle valve. Inside the growth chamber, the samples sit on a revolving, heated, disk-shaped holder made of SiC-coated graphite. The overall design allows sample heating to 1000°C. However, the intention is to process at substantially lower temperatures. Due to the large mass and the possible use of the high temperature capability, appropriate heat shielding and water cooling have been installed, as can be seen in the cross-sectional view of the system, shown in Figure 1.
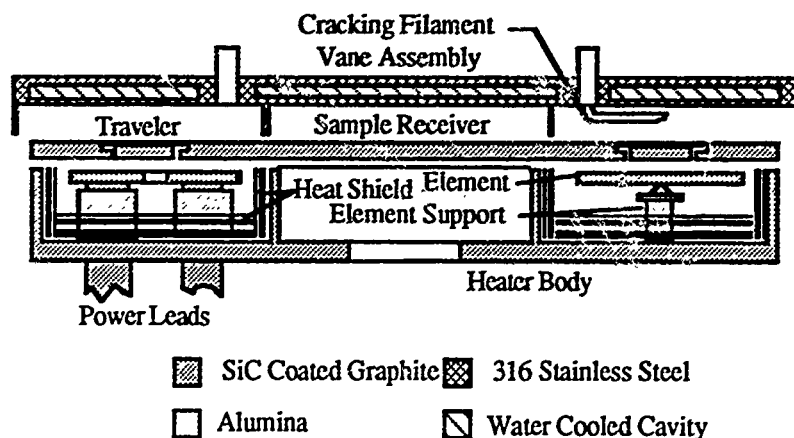

Figure 1.   Cross-sectional view of the ALE growth chamber for the deposition of III-V nitrides.

A specially designed vane assembly allows the deposition in the ALE mode. The assembly is stationary above the rotating susceptor and consists of sixteen separate compartments for the introduction of up to eight different process gases without mixing. As wafers travel under each compartment, they experience a different atmosphere. However, the ALE process requires a purge cycle with an inert gas between each exposure of the wafers to the reactants. This prevents mixing of the reactant gases and allows time for the desorption of physisorbed molecules. After this cycle only the chemisorbed monolayer remains. If a purge is applied after every exposure to reactants, half of the zones (eight) remain for the deposition. That means four zones for each reactant when a binary compound is grown. This

arrangement allows the growth of four monolayers of each element (about 7-10 Å) of the binary compound per revolution of the susceptor. The anticipated growth rate in the ALE mode is about 1 μm per hour. Figure 2 shows a column V compartment containing a tungsten filament for creating active nitrogen containing species from the decomposition of ammonia. These species facilitate reaction with chemisorbed Ga atoms at low temperatures.
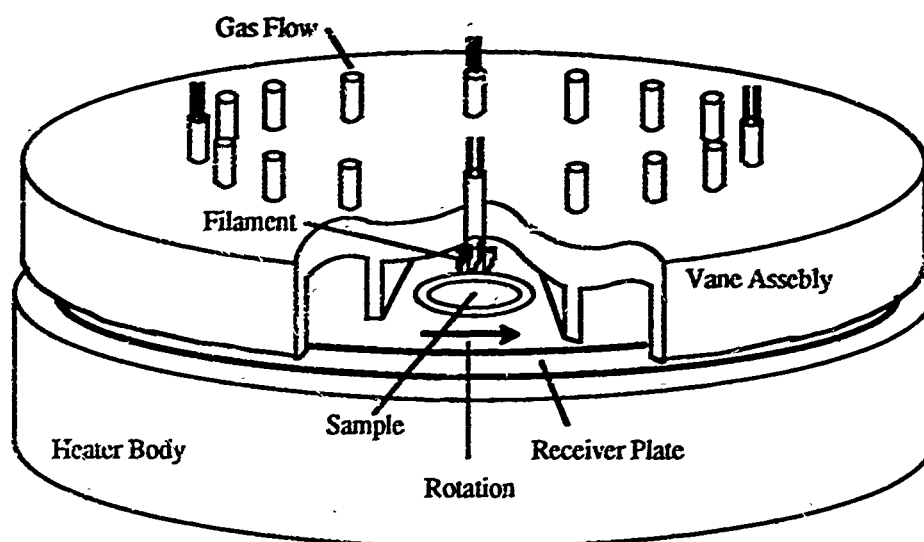

Figure 2.   View into column V compartment. A tungsten filament is used to crack and activate ammonia and thus make it suitable for the reaction at a low temperature.

The gas introduction system is capable of handling organometallic and gaseous precursors. All gases used in the deposition are ultra high purity and further purified by chemical purifiers. Each OM module consists of a bubbler sitting in a constant temperature bath, a capacitance pressure transducer for measuring the pressure inside the bubbler, a manual metering valve for the pressure control, a mass flow-rate controller for the carrier gas, and several manual and pneumatic shut-off valves. This hardware allows precise dosing of the OM into the reaction chamber via the control of three key parameters: bubbler temperature, bubbler pressure and the carrier gas flow rate. Since the partial pressure of the OM in the bubbler depends on the temperature only, one can calculate the volume ratio between the OM source and the carrier gas supplied into reaction chamber simply as the ratio between the partial pressure of the OM at the bubbler temperature, $p_{OM(T)}$, and the partial pressure of the carrier gas $(p_T - p_{OM(T)})$.

$$X_{OM(T)} = \frac{p_{OM(T)}}{p_T - p_{OM(T)}}$$

The exact number of moles of OM reactant introduced into chamber is then calculated from the known flow rate of the carrier gas. The control of the introduction of the gaseous sources includes only a mass flow controller with a shut-off valve.

4

2. Growth Theory

Several different inorganic and organic precursors have been considered for the ALE of GaN. Organometallics were chosen over chlorides for the source of Ga because of high purity, ease of transport from the source to the chamber, and excellent control over dosing. Triethylgallium was chosen over trimethylgallium for two reasons: (1) lower decomposition temperature and thus lower growth temperature, which would reduce the concentration of nitrogen vacancies, and (2) cleaner surface reaction (the decomposition of trimethyl species often results in the decomposition of the higher deposition methyl radical resulting in residual C atoms which become incorporated in the growing film). Ammonia was chosen over hydrazine and nitrogen fluoride mainly because of safety considerations and cleanliness. Ammonia is available in research grade purity. Moreover, chemical ammonia purifiers, which effectively remove remaining water, oxygen and carbohydrides, are also available.

The reaction energy budget these precursors offer theoretically favors the self-limiting ALE deposition of III-V nitrides on (0001) surfaces of wurtzite or (111) surfaces of zincblende substrates. The growth direction is crucial, because the number of bonds a particular species makes on the surface varies greatly with the growth direction. A constituent of a tetrahedrally bonded compound can make one surface bond in the $(000\bar{1})$ direction, two surface bonds in (1011) direction and three surface bonds in (0001) direction.

An estimate of whether a reaction is favored or not, can be made by comparing the bond energies of the reactants and products. The bond energies between Group III metals and nitrogen, calculated using different methods, are summarized in Table I. For example, suppose, the (0001) surface is terminated with $Ga(C_2H_5)_2$ which makes one bond with the underlaying nitrogen. The subsequent exposure of these adsorbed species to ammonia causes a surface reaction to occur, if making three bonds with Ga is energetically favorable for the ammonia molecule. The process will end with a hydrogen terminated surface which does not react further with ammonia. The bond energy between Ga and the ethyl radical is 57 kcal/mol, and the average bond energy between nitrogen and hydrogen is about 90 kcal/mol.

Table I. Bond energies between III metals and nitrogen obtained by different methods.

B - N	Al - N	Ga - N	In - N	Remarks
115	125	108	105	Pauling's formula [6]
94	90	65	54	Geometrical mean with correction [6]
83-193	52-122	55-85	47-67	Immediate neighbors
72-91	64-80	55-69	49-61	Periodic behavior
66	67(81)	50(56)	49	Heat of vaporization [7]
87	94	69	58	Heat of formation [8]
85±5	75±5	65±5	55±5	Suggested values

Thus, the total enthalpy to break the necessary bonds within the precursors is $(3 \times 57) + (2 \times 90) = 351$ kcal/mol. On the other hand, the enthalpy of formation of each N-Ga bond releases 65 kcal/mol, and the reaction $C_2H_5 + H \rightarrow C_2H_6$ produces about 100 kcal/mol. Thus, the total enthalpy of reaction is: $3 \times 65 + 2 \times 100 = 395$ kcal/mol. Since the energy of reaction is larger than the decomposition energy, the overall reaction to form a H-terminated N-Ga bilayer is favorable.

A similar calculation can be done for the next Ga layer. The Ga cycle starts with a hydrogen terminated nitrogen surface. Arriving TEG chemically adsorbs onto the surface by breaking one H-N bond (90 kcal/mol) and one Ga-ethyl bond (57 kcal/mol) and making one Ga-N bond (65 kcal/mol) and one C-H bond (100 kcal/mol) producing C_2H_6. The energy balance is 147:165 and the reaction is favorable for the deposition of a Ga layer.

The same calculation is valid also for AlN and BN. The only III metal with a marginal outcome is In, as can be seen from the data in Table I. However, such calculations offer only a rough estimate, since (1) data on bond energies are often inaccurate and (2) the enthalpy of transformation from the gas to solid state has been neglected. Energy requirements on a surface which acts as a catalyst may be even lower.

Figure 3 details the ALE process for gallium nitride from triethylgallium and ammonia as it occurs in our system. A clean, oxide-free 6H- SiC surface (A) is exposed to TEG which undergoes chemisorption involving rupture of some of the Ga-C_2H_5 bonds (B) until a continuous layer of adsorbed species is formed (C). Subsequently, the samples are exposed to an ammonia flux flowing across a hot filament (D). The ammonia attaches to the gallium precursor, replacing any previous termination until a complete layer of the NH_2 radical forms as shown in (E) At this point the sample may be again exposed to the TEG and the complete process repeated (F).

3. Growth and Analysis Procedures

In order to test and characterize the new equipment and the overall process, several deposition runs were made using different growth parameters. Table II gives the ranges over which the various parameters were varied. Throughout the test depositions four of the sixteen zones were used for TMG, four for ammonia and eight for the hydrogen purge gas.

Reflection High Energy Electron Diffraction (RHEED) was used to determine the crystallinity and structure of the grown films. Scanning Auger microscopy (JEOL JAMP-30) was performed to determine the presence of impurities and the nominal composition of the GaN layers. The surface morphology of the films was characterized using scanning electron microscopy (Hitachi S-530). Film thickness was measured by using a Rudolph automatic ellipsometer.
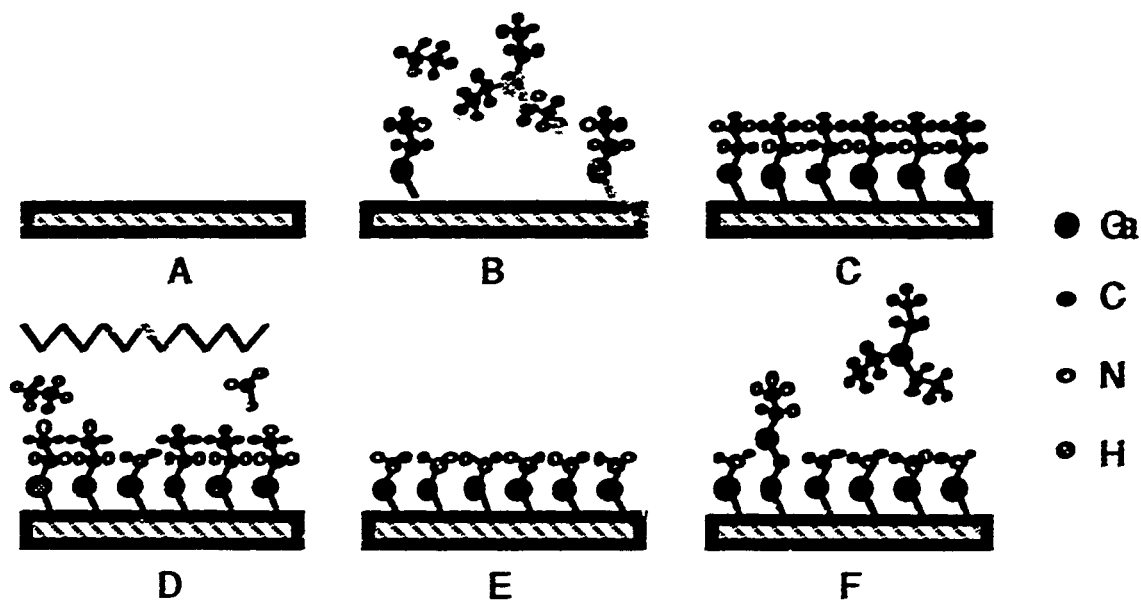
Figure 3. Schematic presentation of GaN ALE process using TEG and ammonia.

Table II. Growth parameters.

Growth temperature	350 - 650°C
Growth pressure	0.5 - 50 Torr
Ammonia flow rate	100 - 300 sccm
H_2 (purge) flow rate	200 - 300 sccm
H_2(OM carrier) flow rate	50 - 100 sccm
TEGa bubbler temperature	-10 - 20°C
TEGa bubbler pressure	400 - 800 Torr
Rotation speed	1 - 2 RPM

C. Experimental Results and Discussion

1. Surface Morphology

Initially, a few CVD runs were attempted, where all reactants were introduced into the same growth zone. The substrate temperature range was, 750-850°C. This did not result in the growth of GaN films. Only large (>10 μm) individual GaN crystals were observed on the surface. These were a possible result of homogeneous nucleation in the gas phase.

After a few unsuccessful experiments, the reactants were separated and distributed to the different growth zones. Substrates were rotated and sequentially exposed to different reactants. Films were grown at a constant chamber pressure of 50 Torr. The other parameters of growth temperature, flow rate, and substrate rotation speed (exposure time to each reactant gas) were changed.

7

Three dimensional growth was obtained at temperatures higher than 600°C, where individual crystallites were clearly seen. All of them had either a hexagonal or a triangular shape, both of which indicated a hexagonal structure. All of them were oriented in the same direction. The {0001} planes were perpendicular to the surface and the {1010} planes of the individual crystallites were parallel to each other. This indicated a good epitaxial relationship with the α(6H)-SiC substrate.

Films grown at temperatures lower than 400°C were continuous with no detectable surface morphology. Figures 4 and 5 show the surface morphology of three GaN films grown under different Ga exposures at 390°C. The film shown in Figure 4 is continuous, as confirmed by chemical analysis. The ovals on the surface of the film are conglomerates of unreacted gallium. Apparently TEG decomposes at this temperature effectively; however, the concentration of ammonia is insufficient for complete reaction. When the supply of TEG was reduced by about three times, a clean GaN film without Ga precipitates was obtained, as shown in Figure 5. However, this procedure also reduced the growth rate from 2000 Å/hr to 600 Å/hr.

2. Chemical Analysis

Scanning Auger microscopy was performed on the samples to determine the presence of impurities and the nominal composition of the GaN layers. Figure 6 shows an Auger spectrum taken from the untreated growth surface. The oxygen and carbon peaks are due to surface oxidation and contamination upon exposure to the atmosphere. No other contaminants were observed within the resolution of the instrument (typically ≈ 0.1 at.%).

An Auger depth profile was also obtained and is shown in Figure 7. The profile shows that indeed the oxygen and carbon contamination was only on the surface. The apparent low nitrogen content of the film is in part due to the relative elemental sensitivity factors. Another factor may possibly be a result of the sputtering action of the 3 kV Ar+ ions. A similar effect has been seen in InN[9].

3. Electron Diffraction

Reflection high-energy electron diffraction (RHEED) was performed on the the GaN films. Films grown at 380°C or higher showed a distinct diffraction pattern indicative of the wurzite structure. Diffraction patterns of a film grown at 390°C and taken in two different directions are shown in Figure 8. Although Kikuchi lines were observed which are the fingerprint of good crystallinity, the surface of the film appears to be rough, as shown by the spotty diffraction pattern.
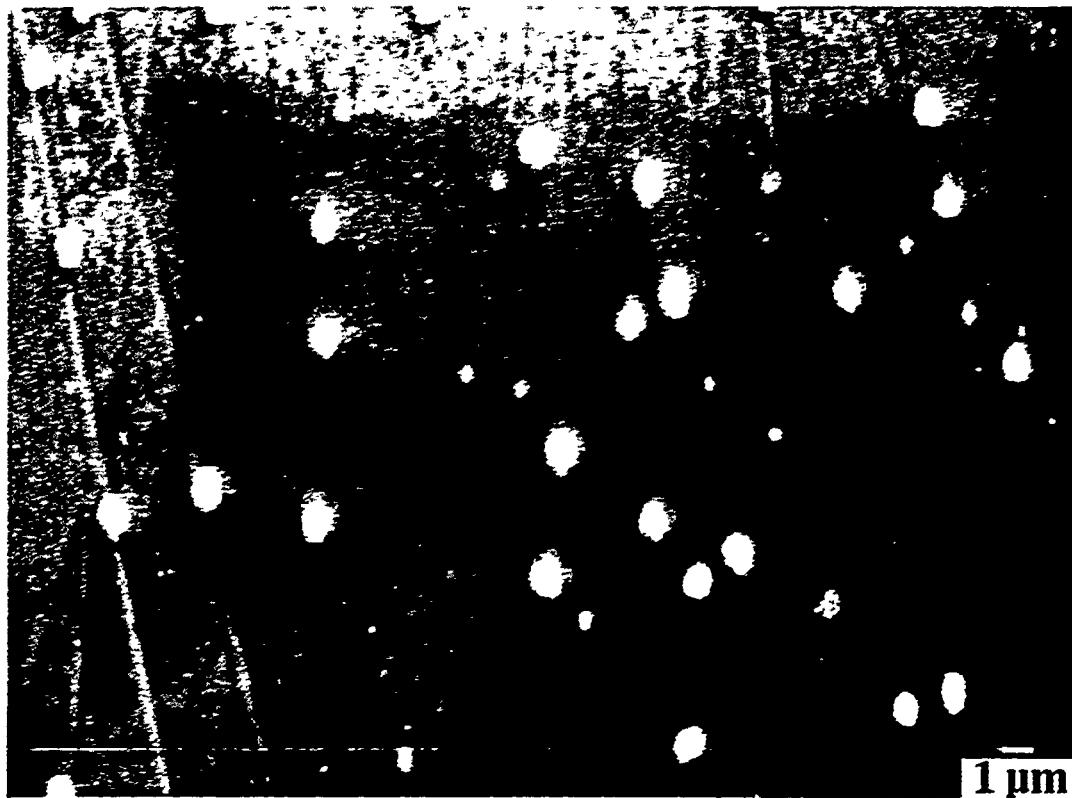
Figure 4. A micrograph of GaN film grown at 390°C on α-SiC. Film is continuous, but there is excess Ga on the surface.
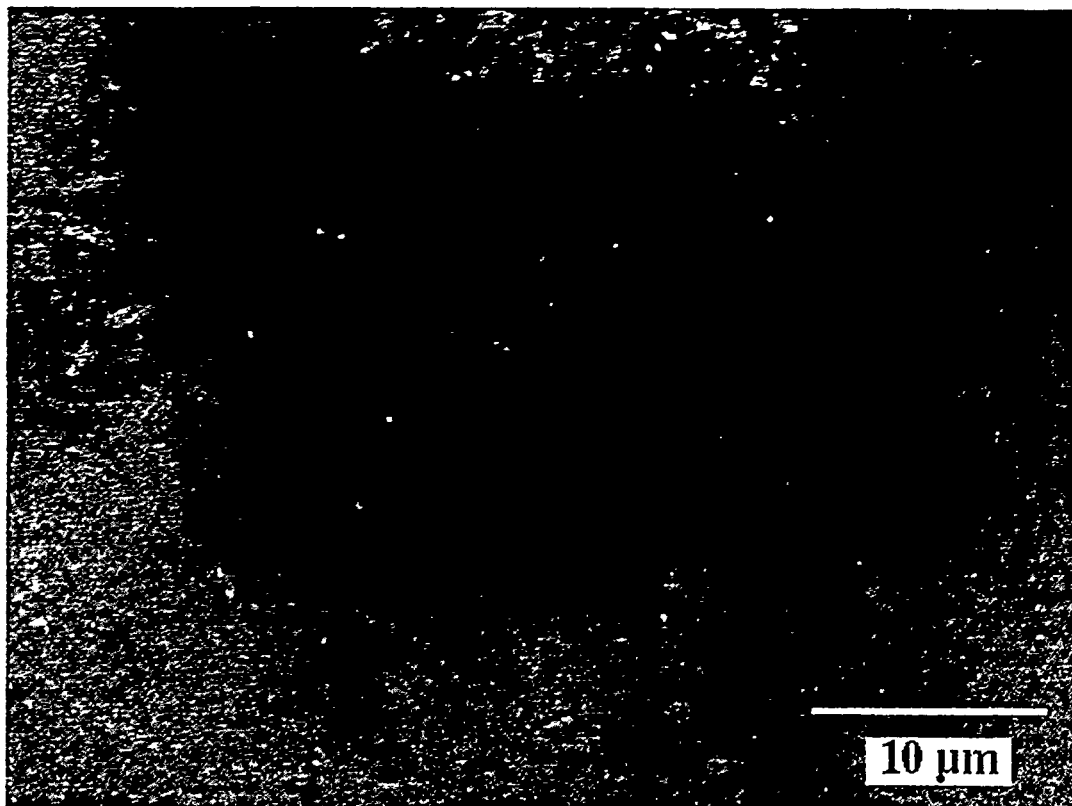

Figure 5. The surface of an as grown ALE GaN film, after TEG flow rate was reduced. No excess gallium was observed on the surface and RHEED showed good crystallinity.
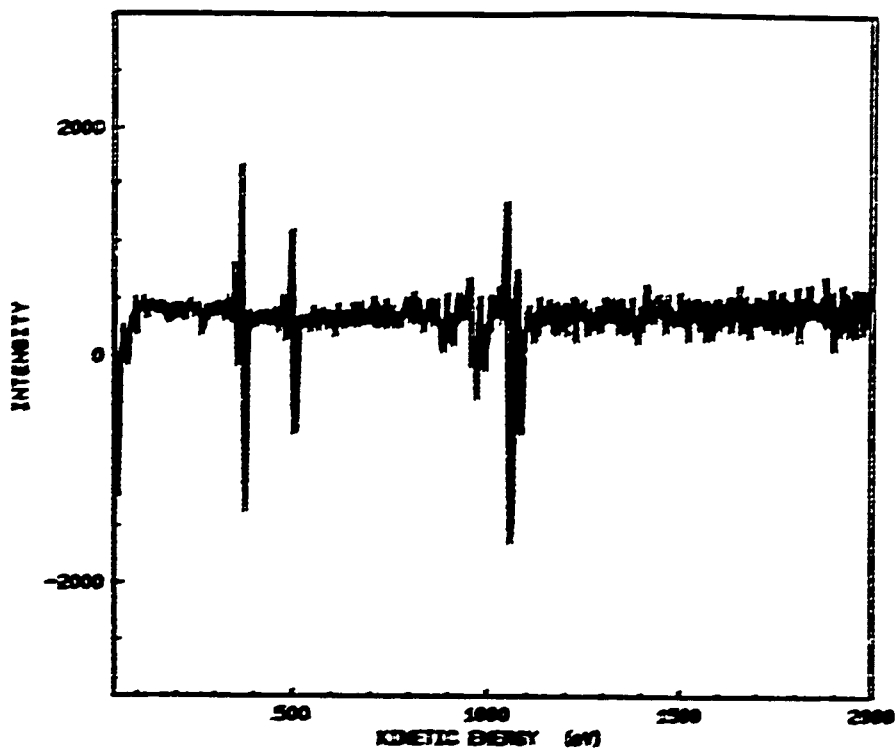
9

Figure 6. Auger spectrum taken from the untreated GaN surface. Only oxygen and carbon contamination was detected, which is due to exposure to the atmosphere.
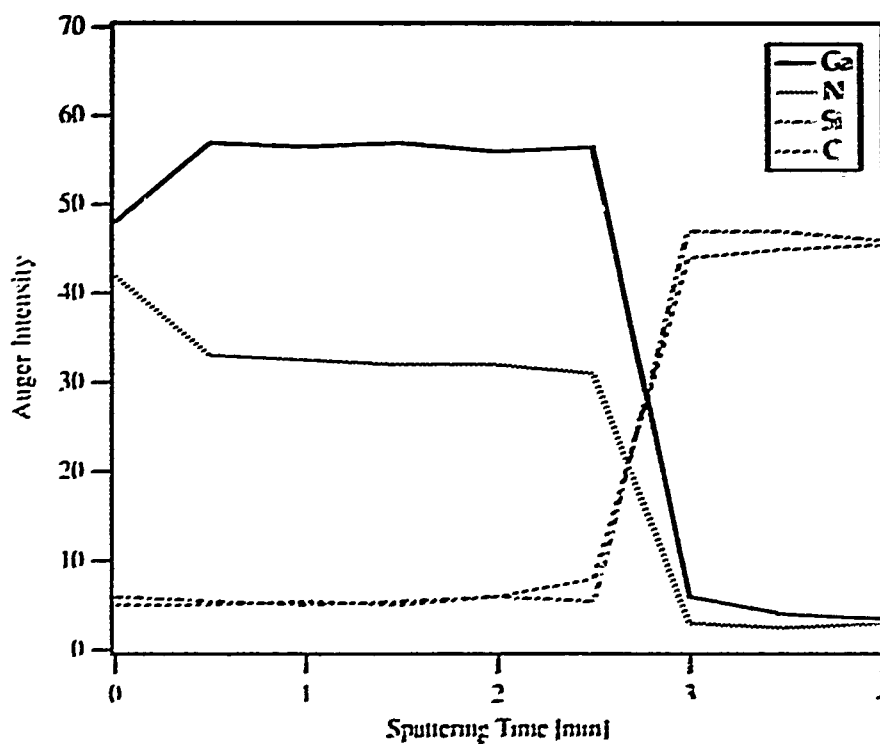

Figure 7. Auger depth profile of GaN on α-SiC (0001). Oxygen and carbon contamination was detected only at the surface.
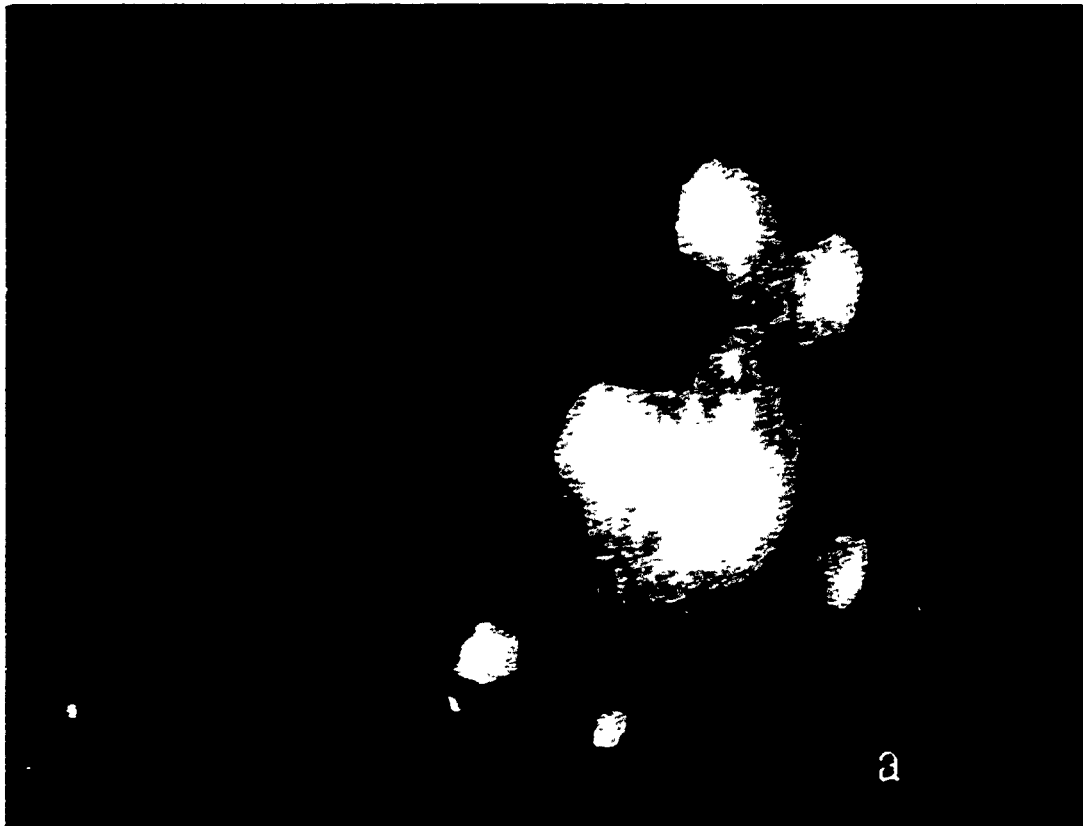
Figure 8. RHEED pattern of a GaN film grown on (0001) a-SiC by ALE. a) $[01\bar{1}0]$, b) $[2\bar{1}\bar{1}0]$

One of the primary objectives of this research was to determine the experimental window in which GaN grows in a truly self-terminating process. Figure 9 shows the dependence of the amount of film grown per cycle with respect to the residence time per reaction zone. One can see that the growth per cycle initially increases quickly with exposure time but becomes more gradual after ≈10 sec. of exposure. Although these growth conditions could be utilized for layer-by-layer growth by correctly adjusting each exposure time, the process was not self-terminating at this temperature. Subsequently, GaN films were grown at a sample temperature of 280°C. The crystallinity of these films has been confirmed by crystal x-ray diffraction. At an exposure time of 22 seconds, the growth rate corresponded to 2.62 Å per cycle, which corresponds to one monolayer of molecular coverage. When the growth was performed with an exposure time of 11 seconds the coverage per cycle falls to 1.2 Å per cycle. Recent mechanical difficulties with the system have prevented us from repeating the run for exposure times greater than 22 seconds, in order to determine if the coverage per cycle will remain unchanged at one monolayer per cycle.
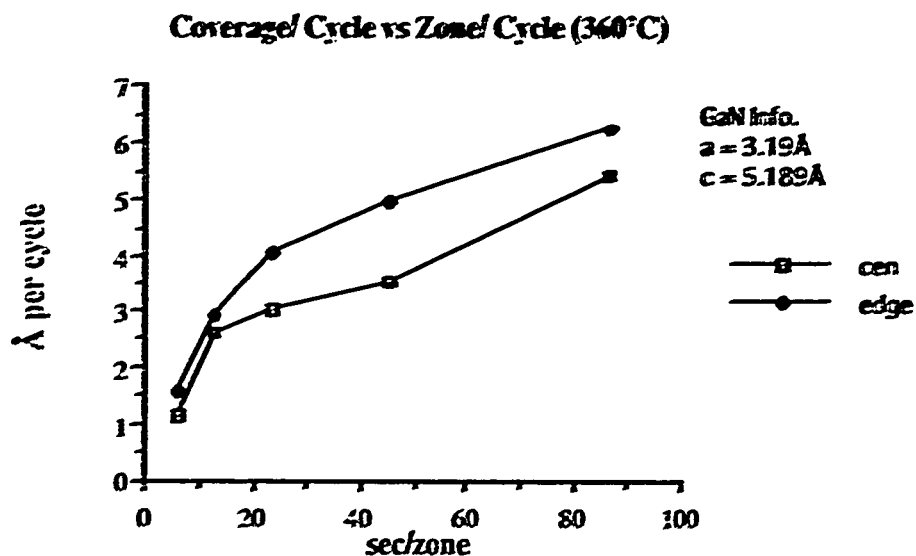
Coverage/ Cycle vs Zone/ Cycle (360°C)

Figure 9. Dependence of the amount of film grown per cycle with respect to the residence time per reaction zone at a growth temperature of 360°C.

D. Conclusions

The first results of the ALE growth of GaN are very encouraging. The system has performed well, and very low temperature growth of GaN has been achieved. The films were chemically stoichiometric crystalline and with a very smooth surface. Details of this part of the research can be found in the Semi-annual Letter Reports for July 1990 and June 1991 and the Annual Letter Reports December 1990 and 1991.

E. References

1. T. Sannoia and J. Arson, U.S. Patent 4 058 430, Nov. 15 (1977).
2. C.H.L. Goodman and M.V. Pessa, J. Appl. Phys. **68**, R65 (1986).
3. S.M. Bedair, M. Tischler, T. Katsuyama, N.A. El-Masry, Appl. Phys. Lett. **47**, 51 (1985).
4. J. Nishizawa, H. Abe and T. Kurabayashi, J. Electrochem. Soc. **132**, 1197 (1985).
5. R. C. Weast ed., *Handbook of Chemistry and Physics*, 69th Edition 1988-1989, CRC Press, Inc., Boca Raton, Florida.
6. L. Pauling, *The Chemical Bond*, Cornell University Press, N.Y., 1967.
7. V. I. Vedeneev, *Bond Energies, Ionization Potentials and Electron Affinities*, St Martin's Press, N.Y., 1966.
8. T. L. Cottrel, *The Strengths of Chemical Bonds*, Butterworths Scientific Publications, London, UK, 1954.
9. C. P. Foley and J. Lyngdal, J. Vac. Sci. Technol. A5, 1708 (1987).

13

III. AlN/GaN Superlattices Grown by Gas Source Molecular Beam Epitaxy

A. Introduction

Commercialization of light emitting optoelectronic devices in the previous decade stimulated considerable interest in those III-V nitrides which possess a direct energy gap in the UV region of the spectrum. A comprehensive review regarding the thin film and optoelectronic research in GaN prior to 1988 has recently been published [1]. Depositions of AlN and AlGaN have also been studied [2,3].

Bandgap engineering in the range of 3.4-6.2 eV can be achieved either by solid solutions or by superlattices of GaN and AlN. The latter are favored for several reasons. As has been shown for the GaAs/GaAlAs system [4,7], optoelectronic devices using multi-quantum well structures instead of heterostructures exhibit lower threshold current density, lower non-radiative recombination rate, narrower emission spectra and reduced sensitivity to temperature. The lattice parameter mismatch between AlN and GaN is only 2.5%, thus layered structures of these two materials offer a way of producing high quality, low dislocation density GaN- and/or AlN-based materials and devices. To our knowledge, superlattices of these two materials (or any other wurtzite semiconductor) have not been produced prior to this investigation. These are also the first semiconducting superlattices exhibiting band discontinuity well above 1 eV.

The following sections describe the procedures used to deposit and characterize the layered structures as well as detail the results and conclusions of this research.

B. Experimental Procedures

The growth system was a modified Perkin-Elmer 430 MBE system. Standard effusion cells were used for the evaporation of Ga and Al, while the nitrogen was activated in a small, MBE compatible, ECR plasma source [8].

Growth studies were conducted on (0001)-oriented α-SiC (6H polytype) and (0001) oriented epitaxial quality sapphire substrate wafers, both of which have a hexagonal structure. All substrates were cleaned to remove organic and metallic contaminants using the following sequence of chemicals, temperatures and times: 1:1:5 solution of $HNO_3:H_2O_2:H_2O$ at 75°C for 5 min, DI water rinse for 1 min, 1:1:5 solution of $HCl:H_2O_2:H_2O$ at 75°C for 5 min and DI water for 5 min. The α-SiC wafers were subsequently oxidized in flowing dry oxygen at 1200°C for 1.5 hrs in order to consume an ≈50 nm thick surface layer of the wafer which contained polishing damage. To remove this oxide layer the substrates were etched for 1 min in 49% HF and rinsed in DI water prior to loading into the MBE system. These last two chemical procedures were also

performed on the sapphire wafers. All substrates were then mounted on a standard 3 inch molybdenum block with indium which provided both good adherence and thermal contact.

The substrates underwent an initial low temperature ($\approx$70°C) outgasing in the load lock followed by slow heating in the transfer tube to a maximum of 900°C with a dwell time of 30 min at this temperature. After cooling, the samples were introduced into the growth chamber and examined by reflection high energy electron diffraction (RHEED) using a 10 kV beam. The resulting RHEED patterns on both the α-SiC and sapphire substrates showed Kikuchi lines indicative of good crystalline quality.

Prior to growth, the substrates were heated to the desired deposition temperature and subsequently exposed to a flux of plasma activated nitrogen species for about 5 min. No change in the RHEED pattern occurred as a result of this procedure. Following the stabilization of temperatures and fluxes, a 140 nm thick GaN buffer layer was grown followed by 20 to 200 periods of AlN/GaN layers having the thickness for a given deposition in the range of 1.5–40 nm. The growth conditions are summarized in Table I.

Table I. Growth Conditions

Nitrogen pressure	1×10^{-4} Torr
Microwave power	50 W
Gallium temperature	990°C
Aluminum temperature	1120°C
Substrate temperature	400–750°C
Growth rate:	
GaN	$\approx$2.5 nm/min
AlN	$\approx$1.6 nm/min
GaN buffer layer thickness	140 nm
Period thickness	1.5–40 nm
Number of periods	20–200
Total growth time	6–7 hrs

After the total growth sequence was completed, the gallium and aluminum cells and the substrate were cooled, while the nitrogen source remained active. This source was turned off and the growth chamber returned to UHV conditions once the substrate temperature was below 400°C. The sample was again evaluated with RHEED to determine the crystal structure and to obtain an initial estimate of the film quality.

C. Chemical Analysis

Scanning Auger microprobe (SAM) (JEOL JAMP-30) analysis was used to determine the presence of impurities and the nominal compositions of the AlN and GaN layers. Auger

spectra taken from the untreated surface showed oxygen and carbon surface contamination due to exposure of the film to the atmosphere. Figure 1 shows an Auger depth profile taken from a sample with 20 AlN/GaN double layers. The layers of each material were 10 nm thick. The profile indicates well defined layers. The samples with thicker layers also showed well defined and sharp interfaces. The quality of the interfaces could not be confirmed by SAM in the case of very thin multilayers, since the escape depth for Auger electrons is about 4–5 nm and because the depth resolution of the sputtering process, which roughens the surface, is in the same range. The Auger spectra presented in Figure 2 were taken from the fourth AlN and the fifth GaN layers of the sample noted in Figure 1. The spectra indicate nominal AlN and GaN compositions and some mixing of Ga and Al in AlN and GaN layers, respectively. A small amount of interfacial mixing may be present; however, TEM observations (see below) revealed well defined layers and thus indicate that the Auger data exaggerate this phenomenon for the reasons stated above. There is also a trace of oxygen contamination which decreased with the distance from the surface. As such, the oxygen peak may, at least partially, be due to the transfer of surface contaminants to the exposed material by ion beam sputtering. No other contaminants were observed within the resolution of the instrument (typically $\approx$ 0.1 at. %).

D. Structural and Microstructural Analyses

X-ray Rocking Curves. The AlN/GaN layered structures were subsequently analyzed by x–ray diffractometry. The CuK_β line was used instead of filtered CuK_α one to obtain a truly monochromatic x–ray line and, therefore, unambiguous determination of the AlN/GaN period and the crystalline quality of the superlattices produced in each deposition. The spectra were obtained around the expected (0002) reflections for "bulk" AlN and GaN.

A perusal of Figure 3 reveals that the diffraction spectra of the layered structures are much more complex than those for bulk crystals and single thin films. This is to be expected, since the lattice parameters in the direction normal to the layers (in our case (0001)) are different for AlN and GaN. Moreover the lattice parameters perpendicular to the surface depend upon the distortion of the lattice caused by the interlayer strain, and, as such, the diffraction peaks appear at different positions than one would expect from the bulk properties of the materials. The layered structure also introduces additional periodicity in the growth direction which is revealed in the diffraction spectra as well. Finally, the diffraction spectra usually contain a peak from the substrate or the buffer layer which is often much stronger than the superlattice peaks. These superimposed peaks are convenient for the determination of the strain in the layers but make diffraction spectra even more complicated and difficult to read.
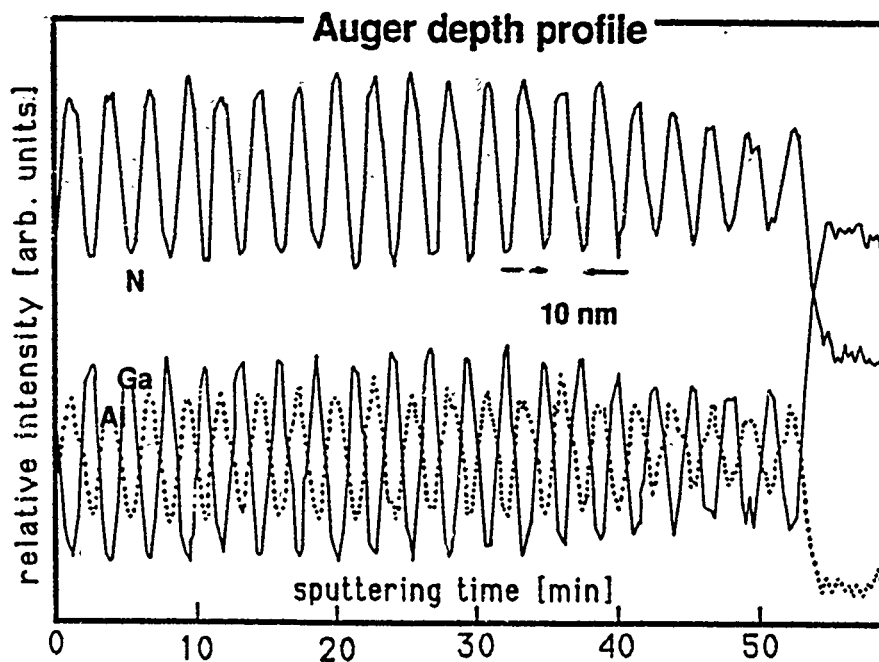
16

Auger depth profile

Figure 1.   Auger depth profile taken from a sample with 20 AlN/GaN double layers. The layers of each material were 10 nm thick.

Auger survey of the fourth AlN layer

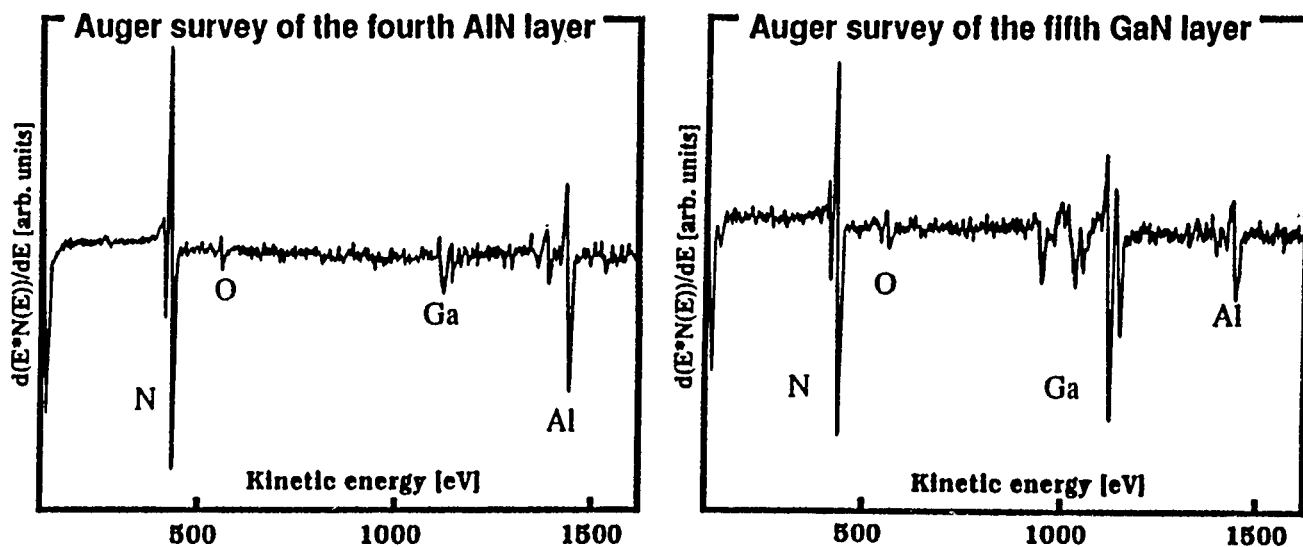**Auger survey of the fifth GaN layer**

Figure 2.   Auger spectra taken from the fourth AlN and fifth GaN layers of the sample noted in Figure 4. The apparent mixing of Al in GaN and Ga in AlN is probably an artifact (see text). Spectra indicate a trace of oxygen contamination.
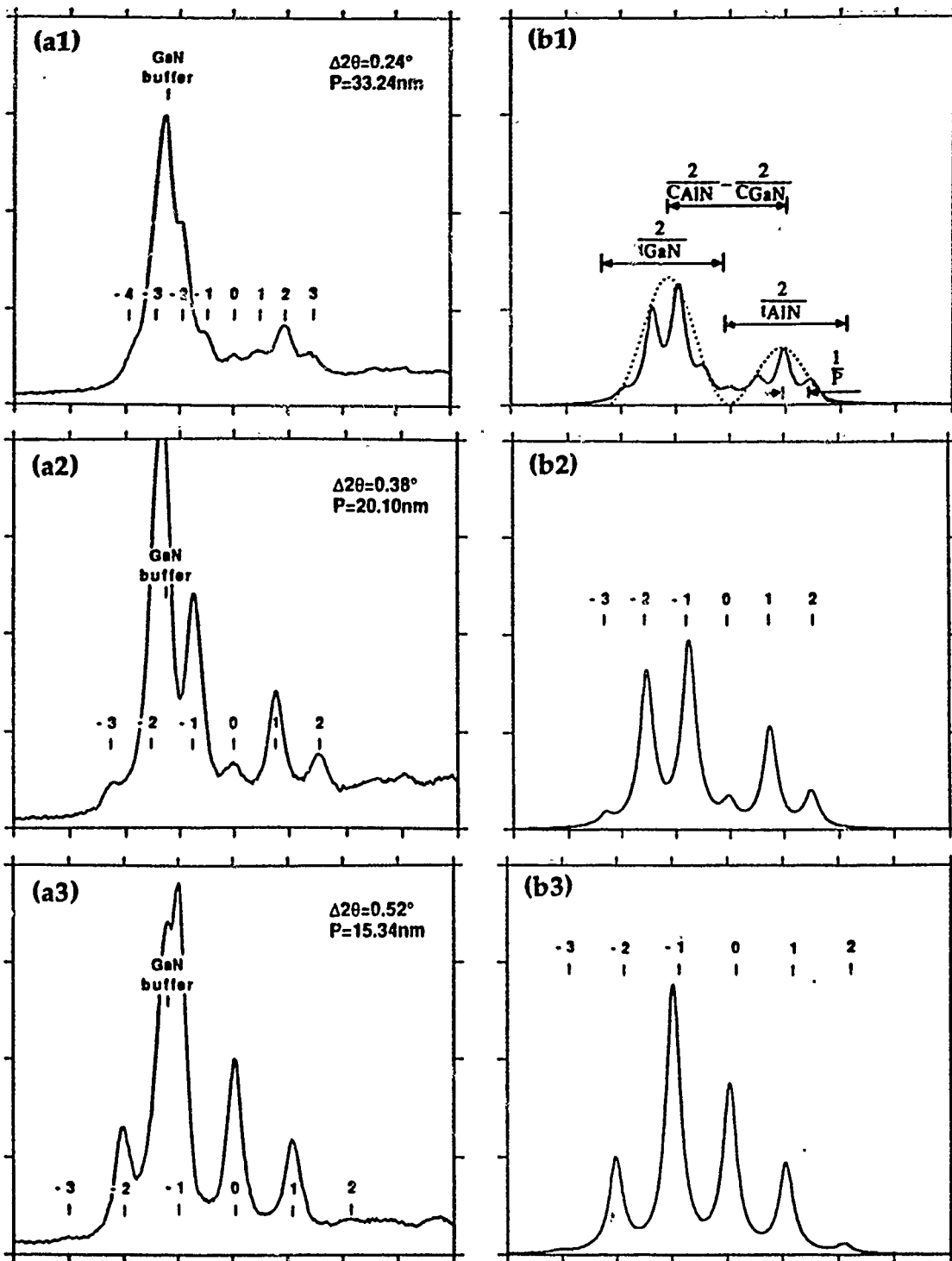
Figure 3. (a) X-ray diffraction spectra of the samples with different periodicities. Each pattern is characterized by the (0002) peak from the GaN buffer layer (marked by "GaN buffer") and a zero-order peak from AlN/GaN layers at $2q = 32°$ (marked by "0") with satellite peaks around it. An angular spacing, $D2q$, of satellite peaks and a calculated bilayer period, P, is given for each spectrum. (b) Diffraction spectra after the subtraction of the GaN buffer layer peak and the overall background. Figure (b1) illustrates the use of the spectra for the determination of different parameters (see text).
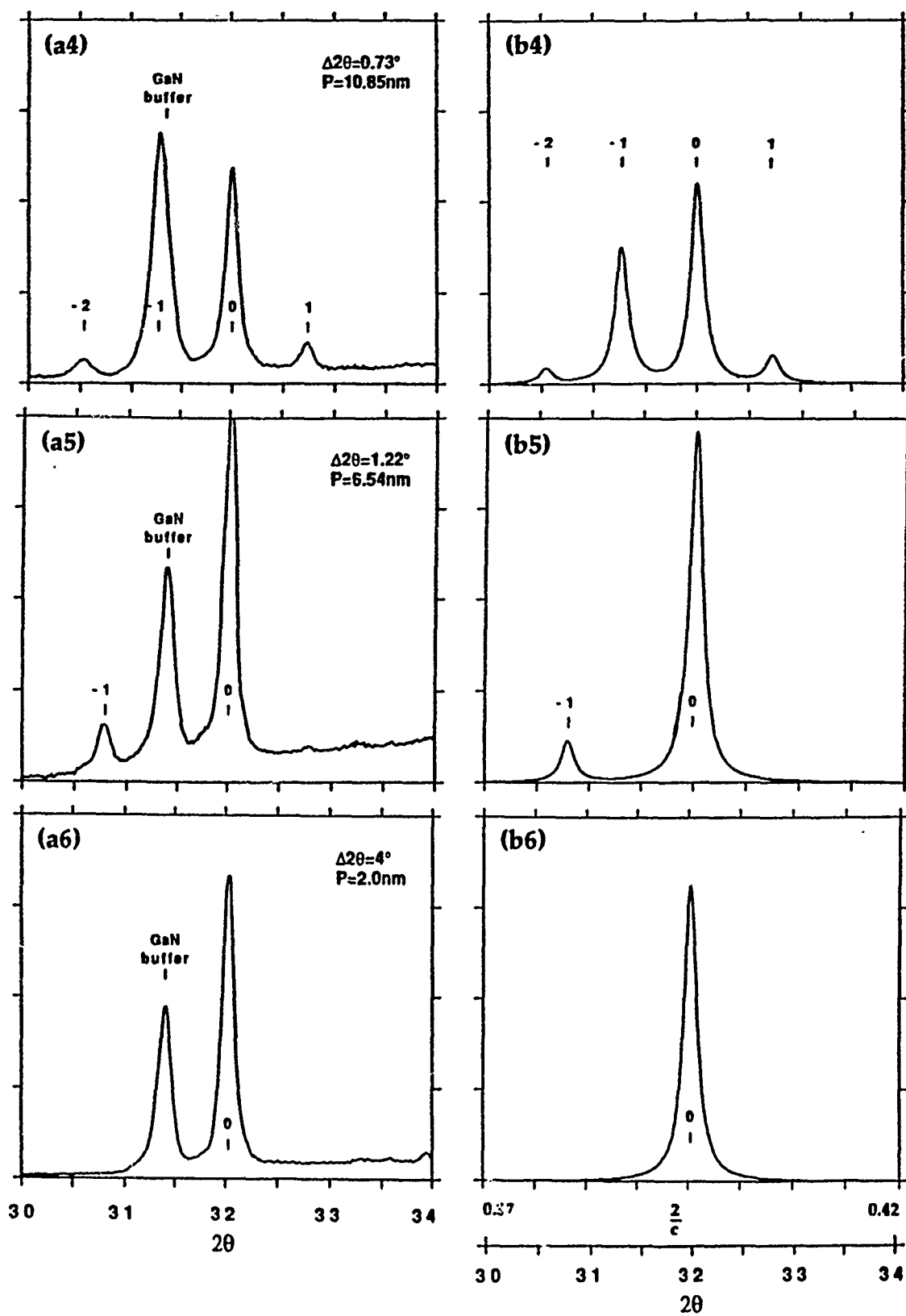
18

Figure 3.   Continued

19

Figures 3(a1–a6) show the evolution of the diffraction peaks as a function of decreasing AlN/GaN bilayer periodicity, P, which is given as

$$P = t_{AlN} + t_{GaN} \tag{1}$$

where t_{AlN} and t_{GaN} are the respective thicknesses of the individual layers of AlN and GaN. Each spectrum shows the (0002) diffraction peak from the GaN buffer layer and the zero order superlattice peak (marked "0"), which represents the average vertical lattice parameter of the superlattice, and associated satellite peaks (marked from -4 to 3). The buffer layer peak is superimposed on the latter peaks making the diffraction from the superlattice unclear. As such, each spectrum in Figure 3(a1-a6) was fitted with a sum of Lorentzian peaks followed by the subtraction of both the buffer layer peak and the overall background, which made the evolution of the peaks with the change of superlattice period easier to visualize. The resulting spectra are shown in Figure 3(b1–b6). In this latter set of spectra, the x-ray intensities are plotted as a function of 2/c, where c is the lattice parameter perpendicular to the surface. This is convenient for measuring parameters (P, t_{AlN}, t_{GaN}, c_{GaN}, c_{AlN}) directly from the spectra.

A representative diffraction spectrum having marked parameters characteristic of a superlattice produced in this study is shown in Figure 3(b1). Several parameters can be determined, as indicated, by measuring reciprocal distances on the spectrum. The periodicity of the superlattice, P, is inversely proportional to the angular spacing of the satellite peaks. The values of t_{AlN} and t_{GaN} can be estimated from the widths of the envelopes (dotted curves) of the AlN and GaN sets of peaks. The perpendicular lattice parameters of the two materials in the individual layers are measured from the angular positions of the envelopes. Finally, the strain in the layered structure can be estimated by comparing the angular positions of the buffer layer peak with the superlattice peaks.

Figures 3(b1) and 3(b2) show two almost completely separated sets of superlattice peaks, each of which represents one of the two materials. Since the envelope widths of the two materials are proportional to $\dfrac{1}{t_{AlN}}$ or $\dfrac{1}{t_{GaN}}$ and their separation scales with $\dfrac{1}{c_{AlN}} - \dfrac{1}{c_{GaN}}$ we have the following condition for the two sets of peaks, taken around the (0002) pole, to be well separated:

$$\frac{2}{c_{AlN}} - \frac{2}{c_{GaN}} > \frac{1}{t_{AlN}} + \frac{1}{t_{GaN}} . \tag{2}$$

For example, if we assume that the lattice parameter perpendicular to the surface for each material has the same value as the bulk (as will be seen later, this is a reasonable assumption for thick layers) and take t_{AlN} equal to t_{GaN}, both sets of peaks are well separated for P>28 nm, which is in good agreement with the measured spectra. In

20

Figure 3(b3) both sets of peaks begin to overlap, and the positions of the two envelopes become less obvious. As one moves toward even shorter periods the two envelopes can no longer be resolved, as their widths become much larger than their spacing. As a consequence of these shorter periods the number of observable satellite peaks decreases. Figure 3(b6), which represents the diffraction spectrum of a superlattice with P=2 nm, shows only the zero–order superlattice peak which is located approximately midway between the expected peaks for pure AlN and pure GaN. The peak corresponds to an interplanar spacing of 0.252 nm, which is intermediate between the spacings of the (0002) planes of AlN (0.249 nm) and GaN (0.258 nm) and represents the average spacing of the (0002) planes in the superlattice. Satellite peaks for this sample are out of the range of the scan, and are expected to be at $\approx 28°$ and $\approx 36°$. As noted above, TEM results show a well defined layered structure; thus, there is no reason to believe that this peak arises from the homogeneous mixing of the two materials.

For superlattices with periodicities over 20 nm (see Figures 3(b1–b2)) the center of GaN envelope coincides with the GaN buffer layer peak. This indicates that both have the same vertical lattice spacings. Since the center of the AlN envelope also appears at the same angular position as one would expect for the (0002) peak of pure AlN, this indicates that individual layers at periods larger than 20 nm have unchanged vertical lattice parameters and thus are relaxed with respect to each other. At periods smaller than 20 nm the positions of the envelopes start changing (compare Figures 3(b2–b3)). This is believed to be related to the lattice distortion due to elastic strain. However, since the overlapping of both envelopes starts at about the same layer period, the quantitative displacements of the centers are not clear, and become even less evident at superlattices with periods smaller than 10 nm (see Figures 3(b4-b6)). In order to more accurately determine the transition between relaxed and strained structures, the reflections from the planes with mixed indices (for example $(10\bar{1}1)$) should be studied.

Transmission Electron Microscopy. Transmission electron microscopy (TEM) (Hitachi H-800) and high resolution microscopy (HREM) (JEOL 200CX) were used to further analyze the AlN/GaN layered structures. Cross-sectional TEM specimens were prepared using standard techniques.

The periodicities calculated from the x-ray spectra were confirmed by the TEM images. Discrepancies between the two methods were found to be less than 5%.

Superlattices grown on α–SiC showed a high degree of crystallinity, which has been confirmed by RHEED, X–ray diffraction, and transmission electron diffraction. Figure 4 shows a TEM image of 5 nm thick layers of AlN and GaN. GaN layers are dark; those of AlN are light. Layers are well defined and have few structural defects. The $(10\bar{1}1)$

diffraction pattern (inset), taken from the layered structure, confirms the monocrystalline nature of the film with a low density of structural defects. The slight waviness of the layers appears to start at the buffer layer; it becomes more defined toward the top of the film. Similar phenomenon has been observed in GaAs/GaAlAs systems and is induced due to the optimum growth temperature difference between the two materials. In the films with thicker AlN/GaN layers this effect is observed as interface roughness between the individual layers, rather than waviness of the layers.
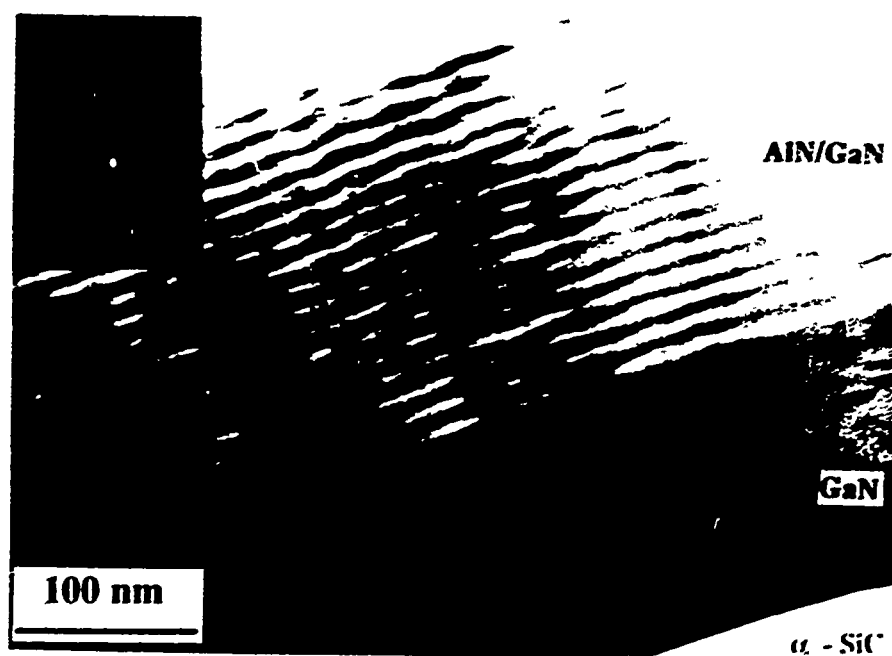

Figure 4.   AlN/GaN layered structure grown on α(6H)-SiC. The thickness of the individual layers is 5 nm.

By contrast, structures grown on sapphire were oriented polycrystalline. These films showed a columnar structure. The range of misorientation of the individual crystallites, measured from the lattice fringes, was found to be from 0° to 8°. However, layers of the two materials within individual crystallites are well defined and no misfit dislocations or other defects have been found. The HREM image of 3 nm thick individual layers indicates perfectly strained material, with uninterrupted lattice fringes at the transitions from one material to the other. Even the structure containing 0.5 nm thick AlN layers (2 monolayers) and 1 nm thick AlN layers (4 monolayers), shows very good compositional contrast between the individual layers.

E. Optical Characterization

The samples grown on α(6H)-SiC were characterized optically by cathodolumines-cence. The spectra were taken at 77 K in the wavelength range of 200 to 800 nm using the excitation electron beam energies of 7 keV.

The bandgap difference between AlN and GaN is almost 3 eV. Thus layers of these two materials produce almost one order of magnitude larger band discontinuities than are achieved in AlGaAs or InGaAs systems. As such, AlN/GaN superlattices may provide some interesting insights regarding the behavior of electrons and holes. For example, they have potential of providing several well-separated confined electronic states.

Spectra taken from the samples with AlN/GaN layer thicknesses of 1/1, 0.5/1, 3/3, and 10 nm/10 nm (0.25 nm ≈ one monolayer) are shown in Figure 5. Each spectrum consists of a broad structure centered around ≈500 nm (2.5 eV), and a well defined peak at a higher energy. The former is due to the luminescence from the α(6H)-SiC substrate.

The higher energy peak increases in energy as the thickness of the layers in different samples decreases. The peak position moves from 3.42 eV for the sample with 10 nm thick wells and barriers, to 4.11 eV for the sample with 1 nm layers. The emission energy from a multi-quantum well structure is expected to also decrease if the well thickness remains constant and the barrier thickness decreases. This effect, which is due to an increase in tunneling probability through thinner barriers, is demonstrated in peaks 1/1 and 0.5/1 which are from structures with 1 nm thick GaN wells and 1 nm and 0.5 nm thick AlN barriers, respectively.

Peaks at higher energies are also expected for AlGaN solid solutions. For example, the emission at 4.1 eV is expected for a molar concentration of Al of 0.32. According to the structural and chemical analyses, there is no reason to believe that a homogeneous solid solution close to this composition had formed. Moreover, random mixing, which may be to some extent present at rough interfaces, would not result in strong, well defined peaks. On this basis, we interpret the high energy peak to be due to the recombination of the electrons and holes confined in the GaN wells. As such, we believe, that the spectra demonstrate the formation of the quantized electronic states.

A computer model for the for the calculation of the band structure of AlN/GaN superlattices has been developed and a comparison between the theory and experiments has been made. Two different cases were examined: 1) The emission energy shift as a function of the layer thickness, while the thicknesses of GaN and AlN layers were maintained equal (i. e. $t_{AlN} = t_{GaN} = \frac{P}{2}$), and 2) emission energy shift as a function of the barrier thickness (AlN), while the well thickness (GaN) was maintained constant at 1 nm.
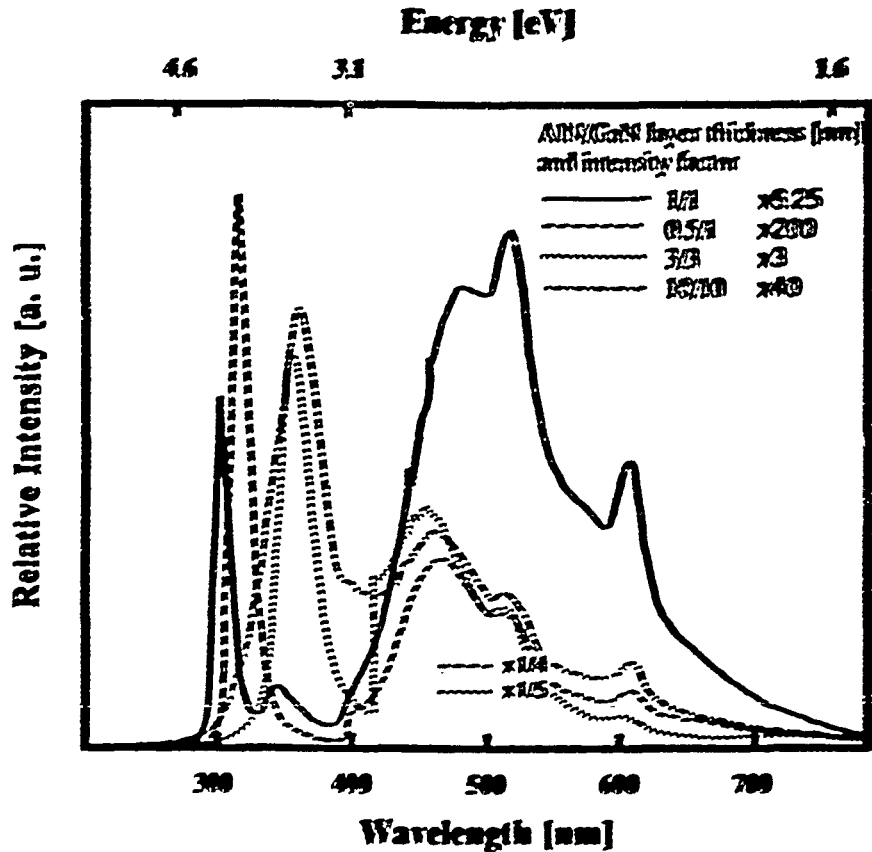
Figure 5: Cathodoluminescent spectra taken at 77K of the AlN/GaN layered structures with different periodicities. Broad peak above 400 nm is due to SiC substrate. High energy peaks are from AlN/GaN layers. Emission energy decreases with increasing GaN well thickness (1/1, 3/3, 10/10) and decreasing AlN barrier thickness (1/1, 0.5/1)

The allowed energy bands for the electrons in the conduction band and for the holes in the valence band in the superlattice were calculated using a one-dimensional Krönig–Penney model. According to this an electron or a hole can occupy a particular energy state in the superlattice only, if the following is true:

$$\left| \cos\left[\frac{t_1(2mE)^{\frac{1}{2}}}{\hbar}\right]\cosh\left[\frac{t_2(2m(V-E))^{\frac{1}{2}}}{\hbar}\right] \right.$$

$$\left. + \left(\frac{V}{E}-1\right)^{\frac{1}{2}}\left(\frac{V}{2E}-1\right)\sin\left[\frac{t_1(2mE)^{\frac{1}{2}}}{\hbar}\right]\sinh\left[\frac{t_2(2m(V-E))^{\frac{1}{2}}}{\hbar}\right] \right| \le 1$$

E is the energy of electrons (holes), V the barrier height (band discontinuity), m the effective mass of the carriers, $\hbar$ the Planck's constant divided by 2π, and t_1 and t_2 are the respective well and barrier widths. Since there is no "hard" value for the effective mass of

24

electrons or holes in AlN and GaN, the average values of the available data were taken. The effective mass of electrons was taken as $0.2m_0$ and that of holes as $0.8m_0$. A conduction and valence band discontinuity was chosen by variation to provide the best fit to the transition energies observed by cathodoluminescence. The best fit was obtained when one half of the total bandgap discontinuity (1.4 eV) was assigned to the conduction band and one half to the valence band. The total bandgap discontinuity was calculated as the difference between the bandgaps of AlN and GaN. For the lack of data on the mechanical properties of semiconducting nitrides, the effect of the biaxial strain on the bandgap shift could not be included in the calculation, although it is expected to have a considerable influence on the bandgap of both materials.

The shaded areas in Figure 6(a) represent the lowest four calculated energy bands for the electrons in the conduction band and the holes in the valence band as a function of the individual layer thickness while the thicknesses of the AlN and GaN were kept equal. The lowest transition energy in the superlattice at a particular layer thickness is obtained as the distance between the lower edge of the first energy band for the electrons and the upper edge of the first energy band for the holes. The arrows indicate the transitions in the structures with 1, 3, and 10 nm thick AlN and GaN layers. The length of the arrows corresponds to the emission energy observed by the cathodoluminescence. The luminescence spectra for mentioned three structures are shown in Figure 6(b). The spectra show sharp and well defined peaks with the energies above the bandgap of GaN. The width of the peaks increases with the layer thickness as the superlattice makes a transition from the pseudomorphic to a relaxed structure. The measured and calculated transition energies for these superlattices are collected in Table II.

TABLE II. Calculated and measured transition energies for different layer thicknesses.

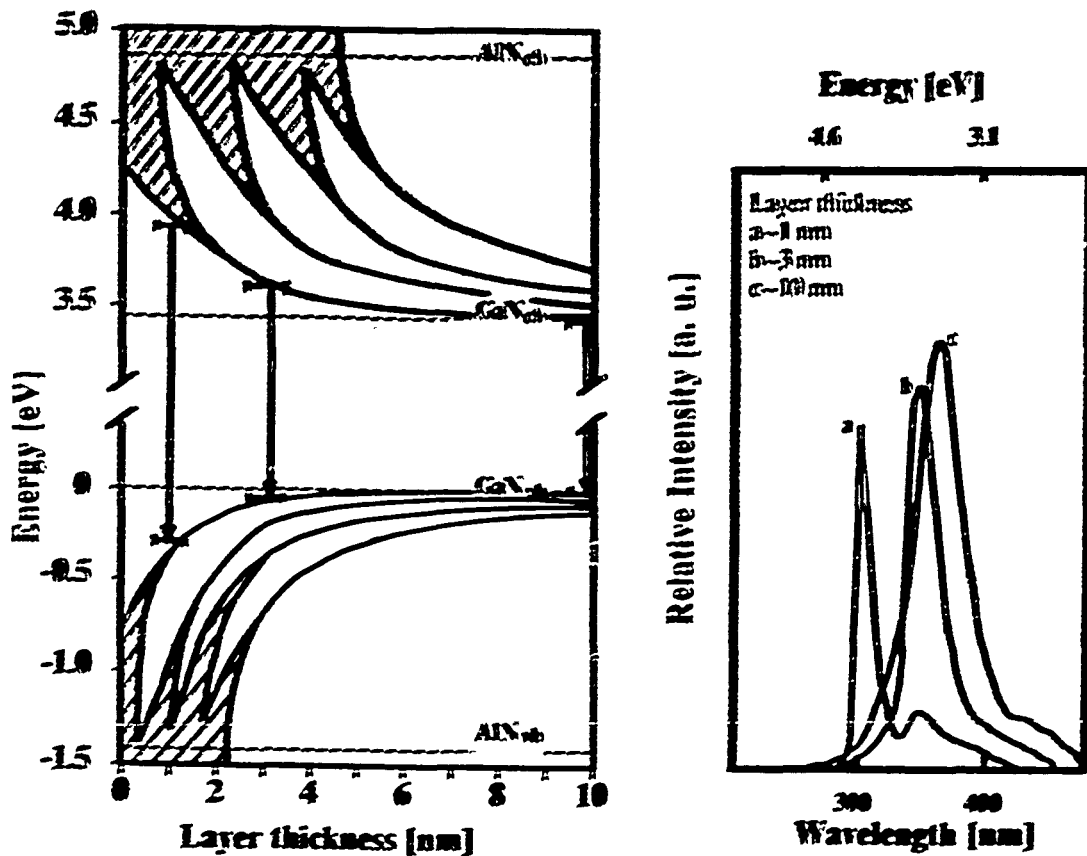| Layer thickness [nm]	$E_{calculated}$ [eV]	$E_{measured}$ [eV]	ΔE [meV]
1	4.29	4.11	180
3	3.64	3.47	170
10	3.42	3.42	≈0

Figure 6: (a) The lowest four calculated energy bands for the electrons in the conduction band and the holes in the valence band as a function of the individual layer thickness while the thicknesses of the AlN and GaN were kept equal. The arrows indicate the transitions in the structures with 1, 3, and 10 nm thick layers, whose cathodoluminescence spectra shown in (b).

Similar to the Figure 6(a), show the shaded areas in Figure 7(a) the lowest two energy bands for the electrons and the lowest three energy bands for holes as a function of the barrier width at a constant well width of 1 nm. The arrows again indicate the measured transition energy of a particular structure. The measured luminescence spectra for 0.5 nm and 1 nm thick barriers are shown in Figure 7(b). The calculated and measured energies are summarized in Table III.
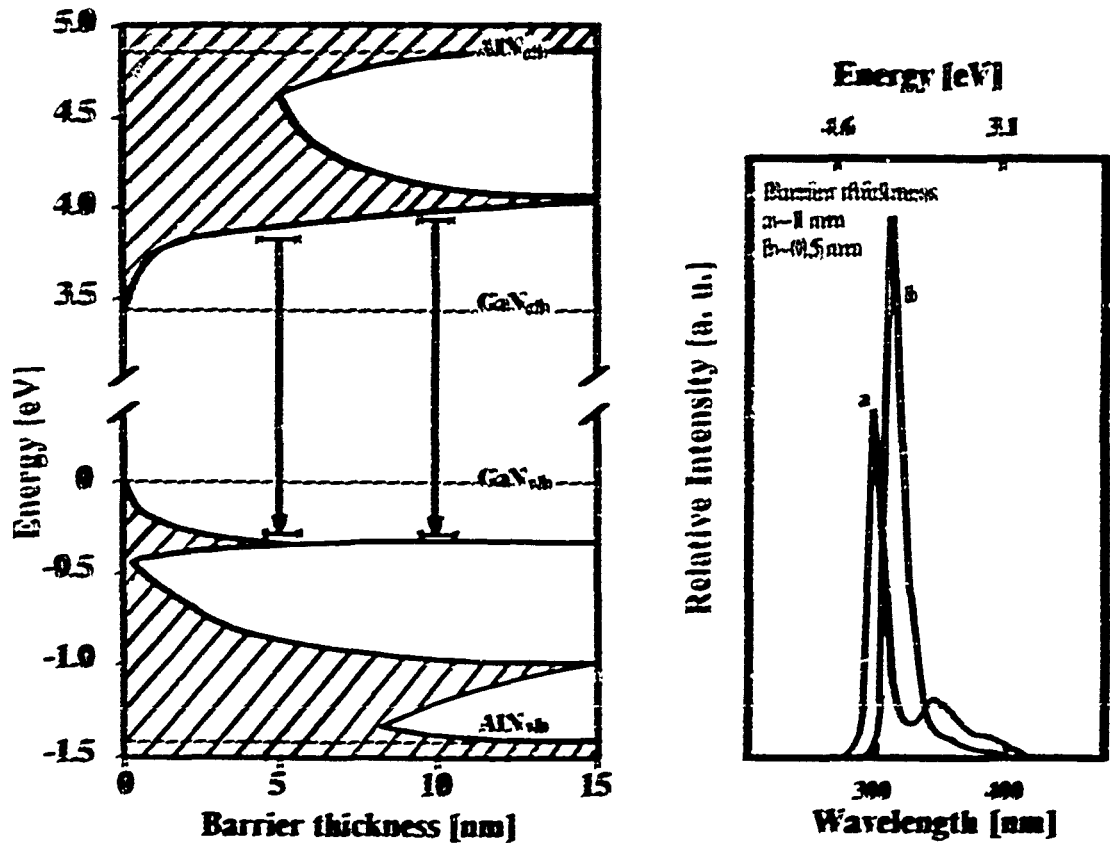
26

Figure 7: (a) The lowest two energy bands for the electrons and the lowest three energy bands for the holes as a function of the barrier width at a constant well width of 1 nm. The arrows indicate the measured transition energy of a particular structure. The measured luminescence spectra for 0.5 nm and 1 nm thick barriers are shown in (b).

TABLE III. Calculated and measured transition energies for different barrier thicknesses.

Layer thickness [nm]	$E_{calculated}$ [eV]	$E_{measured}$ [eV]	ΔE [meV]
0.5	4.19	3.93	260
1.0	4.29	4.11	180

A quick examination of both tables tells us the following facts: 1) The highest transition energy shift observed in this study was above 700 meV and occurred for the superlattice with 1 nm thick barriers and wells. 2) The emission energy shift for the superlattice with 0.5 nm thick barriers was slightly lower than the value above due to better coupling between adjacent wells (higher tunneling probability due to thinner barriers). 3) There exists an energy offset between the calculated and measured values, which was in the range of experimental error for 10 nm thick layers and increased to 170 meV for thinner layers and even up to 260 meV for superlattices with the thinnest barriers.

The reasons for the observed offset can be several. 1) There exists a possibility that the values for the effective masses used in the calculation are not accurate. For example if the effective masses were larger, one would obtain lower theoretical value for the transition energies and as such also lower offset. 2) The lattice mismatch between AlN and GaN produces strain, which induces bandgap shift in both materials. This shift is expected to be rather high for the materials with 2% misfit (i. e. in the range of ≈100 meV). 3) Interfacial mixing of Al in GaN and Ga in AlN in the monolayer scale could significantly change the transition energy in superlattices having individual layers only a few monolayers thick.

The offset for the moderately thin layers (1 and 3 nm) seems to be fairly constant (180 and 170 meV), which would not be the case if solely an error in the effective masses were in question. The fact, that the offset is negligible for thick layers (layers above the critical thickness, which are relaxed with respect to each other) and almost constant for the layers below the critical thickness (which are biaxially strained) implies the connection between the strain induced bandgap shift and the observed offset. As such luminescence data could be a rough measure whether a layered structure is pseudomorphic or not.

The offset for the superlattices with two monolayer thick barriers is even larger than that of superlattices with moderately thin individual layers for additional 90 meV. This jump, which could not be induced by the strain is most likely the consequence of interfacial mixing, which lowers the barrier height and as such decreases the transition energy. A more sophisticated model, which would include bandgap shift due to elastic strain and also assume one monolayer of interfacial mixing is expected to give much better agreement between the experiment and theory.

F. Summary

Growth and characterization studies of AlN/GaN layered structures have been conducted using a modified gas source MBE technique. Layers as thin as two monolayers have been grown. X-ray and TEM results revealed strained material (no misfit dislocations at the interfaces) for layers thinner than 6 nm and a completely relaxed structure for layers

thicker than 10 nm. Cathodoluminescence studies showed a transition energy shift as high as 700 meV due to the quantum size effect. There exists a constant offset of 170 meV between the experimental and calculated values. Since this offset is present only for the pseudomorphic structures, it has been related to the strain induced bandgap shift of the two materials.

G. References

1. R. F. Davis, Z. Sitar, B. E. Williams, H. S. Kong, H. J. Kim, J. W. Palmour, J. A. Edmond, J. Ryu, J. T. Glass, and C. H. Carter, Jr., Mat. Sci. & Eng. B 1, 77 (1988).

2. P. M. Dryburgh, J. Cr. Growth 94, 23 (1989).

3. Y. Koide, H. Itoh, M. R. H. Khan, K. Hiramatu, N. Sawaki, and I. Akasaki, J. Appl. Phys. 61, 4540 (1987).

4. W. T. Tsang, Appl. Phys. Lett. 39, 786 (1981).

5. M. G. Burt, Electron. Lett. 19, 210 (1983).

6. P. Davson, G. Duggan, H. I. Ralph, and K. Woodbridge, Superlattices and Microstr. 1, 173 (1985).

7. N. Holonyak, Jr., R. M. Kolbas, R. D. Dupuis, and P. D. Dapkus, IEEE J. Quantum Electron. QE 16, 170 (1980).

8. Z. Sitar, M. J. Paisley, D. K. Smith, and R. F. Davis, Rev. Sci. Instr. 61, 2407 (1990).

IV. Luminescence and Lattice Parameter of Cubic Gallium Nitride

A. Introduction

Because of its wide direct bandgap of 3.45 eV and the large predicted electron drift velocity [1], GaN has the potential for near ultraviolet (NUV) and, with the application of suitable dopants, also for short wavelength visible optoelectronic devices as well as transit-time-limited electronic devices.

The wurtzite (w) polytype of GaN has been grown by numerous investigators using various substrates and deposition techniques. However, the primary limitation of high n-type conductivity and the associated inability to achieve p-type character has been universal in the as-grown films. Pankove [2, 3] speculated, that one might be able to surpass apparently inherent problems of GaN by producing the metastable cubic phase, although there is no fundamental argument for that.

Cubic (c) GaN has been previously reported in the forms of cubic dendrites on the hexagonal phase [4], nearly epitaxial films on (100) GaAs [5], and epitaxial films on (100) β-SiC [6], (0001) sapphire [7], (100) MgO [8] and (100) GaAs [9]. Previously reported values of the lattice parameter a_0 were between 0.450 and 0.455 nm [6–10]. Bandgap and the band structure for cGaN was theoretically predicted by Pankove and Bloom [11]. These calculations used a composite of factors known for hexagonal GaN and for other zinc-blende semiconductors such as GaAs. The resulting value was 3.4 eV, which is essentially that of the hexagonal phase. From the analogy of cubic and hexagonal forms of SiC, which is considered a similar material, one would expect cGaN to have a more narrow forbidden gap than the wurtzite polytype. A considerably lower experimental value of 3.28 and 3.30 has been reported for the room temperature bandgap based on luminescence [15] and absorption [8] measurements, respectively.

B. Experimental Procedure

Cubic GaN thin films were grown by a modified gas source molecular beam epitaxy (MBE) technique in the range of 550-650°C. The precursors were metallic Ga and ultra high purity N_2. A standard effusion cell was used for the evaporation of the Ga, while nitrogen was activated/dissociated in a microwave glow-discharge or in an electron cyclotron resonance (ECR) plasma source [13]. Cubic (zinc blende) β-SiC, (100) orientation, chemically vapor deposited on (100) Si wafers, was used as the substrate. The lattice parameter of β-SiC is 0.436 nm, which is only ≈3.5% less than one would predict for cGaN using known values for tetrahedral radii. The growth apparatus and procedures, substrate deposition and surface preparation, as well as the results of chemical and structural analyses of the cGaN films are described in detail in Ref [7].

The in-situ chemical analysis reported below was conducted using X-ray photoelectron spectroscopy (XPS) situated in an UHV chamber connected to the MBE system. X-ray diffractometry, and photo- (PL) and cathodoluminescence (CL) were performed ex-situ. A Philips x-ray diffractometer was utilized for diffraction measurements. Silicon and SiC peaks were used for the calibration of the angular positions of the GaN peaks. Photoluminescence was performed with an Ar^+ laser (Spectra Physics 2035) tuned to ≈ 300 nm. Emission from cathodoluminescence was achieved by 5 keV excitation.

C. Experimental Results

The in-situ XPS results did not reveal carbon or oxygen contamination within the resolution of the instrument (typically 0.1%), as shown in Figure 1. This is in contrast to the results reported for the chemical analyses of our initial GaN thin films, thus the contamination observed previously [16] originated mainly from the exposure of the films to the atmosphere, prior to the analyses.
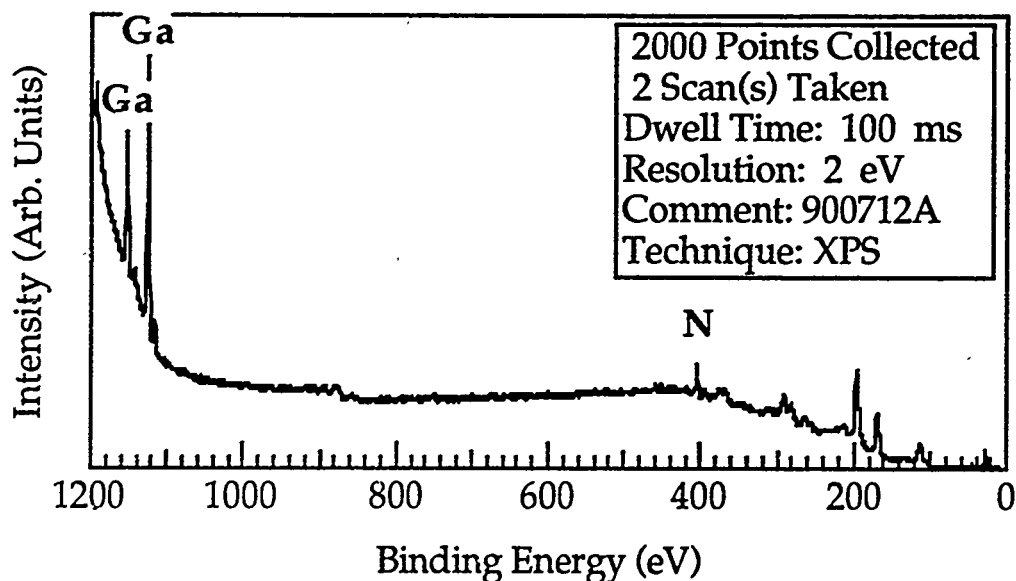
Figure 1. In-situ XPS spectrum of as-grown GaN. Film shows no surface contaminants within the resolution of the technique. The unlabeled low energy peaks are Auger peaks.

From the x-ray data the lattice parameter of cGaN was determined to be 0.451 nm, which is in good agreement with calculated and previously reported values. The resulting x-ray diffraction spectrum is shown in Figure 2. This spectrum also supports the previous analysis [6] regarding the achievement of epitaxial growth, as indicated by the parallel (200) directions of the film and substrate (if they were not, the same low index peaks of the film and substrate would not be observed).

The bandgap determined from the room temperature PL data of wGaN was ≈3.44 eV, in agreement with previously reported values. The measured bandgap of the cGaN showed a considerably lower value: 3.28 eV at room temperature and 3.31 eV at 80K. Photoluminescence revealed a broad featureless peak. The full width at half maximum (FWHM) was 30 nm or 0.13 eV. The high peak width is believed to be caused by the strain due to defects piled up at the heteroepitaxial interface (i.e., dislocations, twin boundaries) [14]. Thus GaN does act similarly to SiC in that the bandgap for the cubic phase is more narrow than that for the hexagonal polytype.
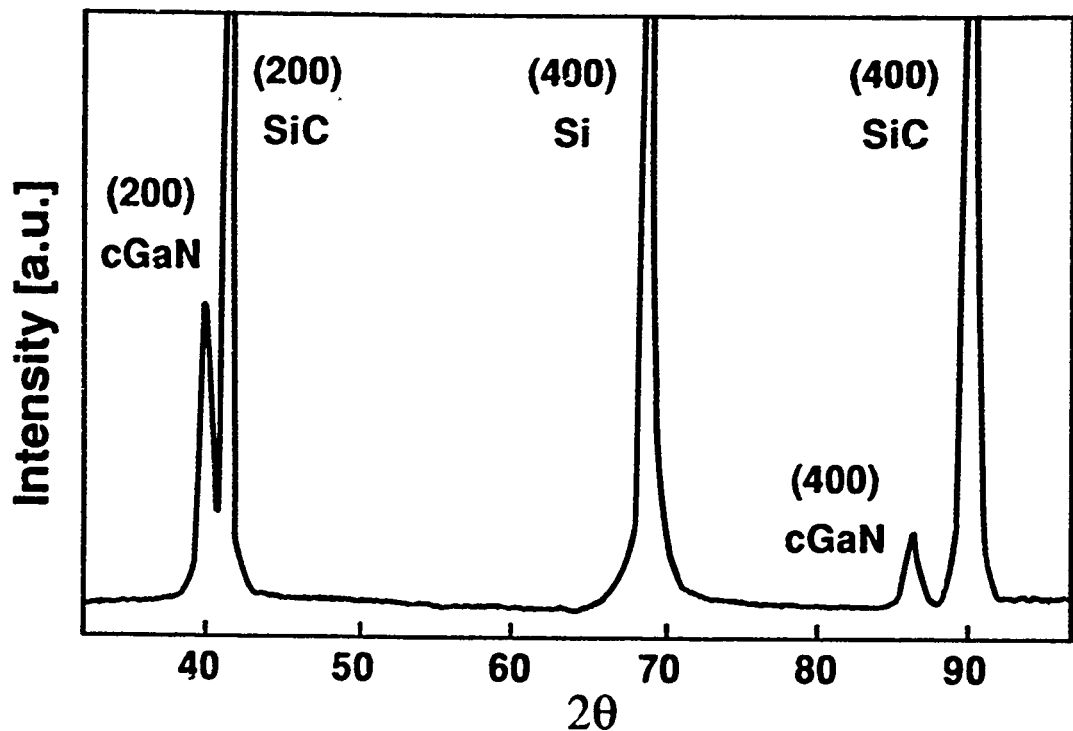
Figure 2.   X-ray spectrum of cGaN grown on (100) β-SiC on Si. Silicon (200) and SiC (200) lines were used for calibration. The lattice parameter of cGaN was determined from these results to be 0.451 nm.

The cathodoluminescence (CL) of a cGaN epilayer at 15K showed a cluster of peaks with a high energy shoulder at ≈3.33 eV, as shown in Figure 3. A perusal of that cluster shows that it consists of five peaks. The four low energy ones are energetically equally spaced. Their spacing was measured, assuming a Gaussian shape for each of them, to be ≈50 meV; their FWHMs ≈45 meV. It is believed that the equal spacing arises from phonon interactions and, as such, the low energy side of the observed cluster consists of a zero phonon peak centered at 3.29 eV and three phonon replicas. The exact nature of the high energy peaks located at 3.33 and 3.29 eV is not known, however, it is believed that they originate due to band-to-band and impurity-to-band transitions, respectively.

The energy of the observed phonons is about 20% lower than the TO phonon energies in wGaN and only half of the values measured for LO phonons [15]. Since data on phonons in cGaN do not exist, a direct comparison could not be made. A concise study of Raman scattering in cGaN should be conducted.
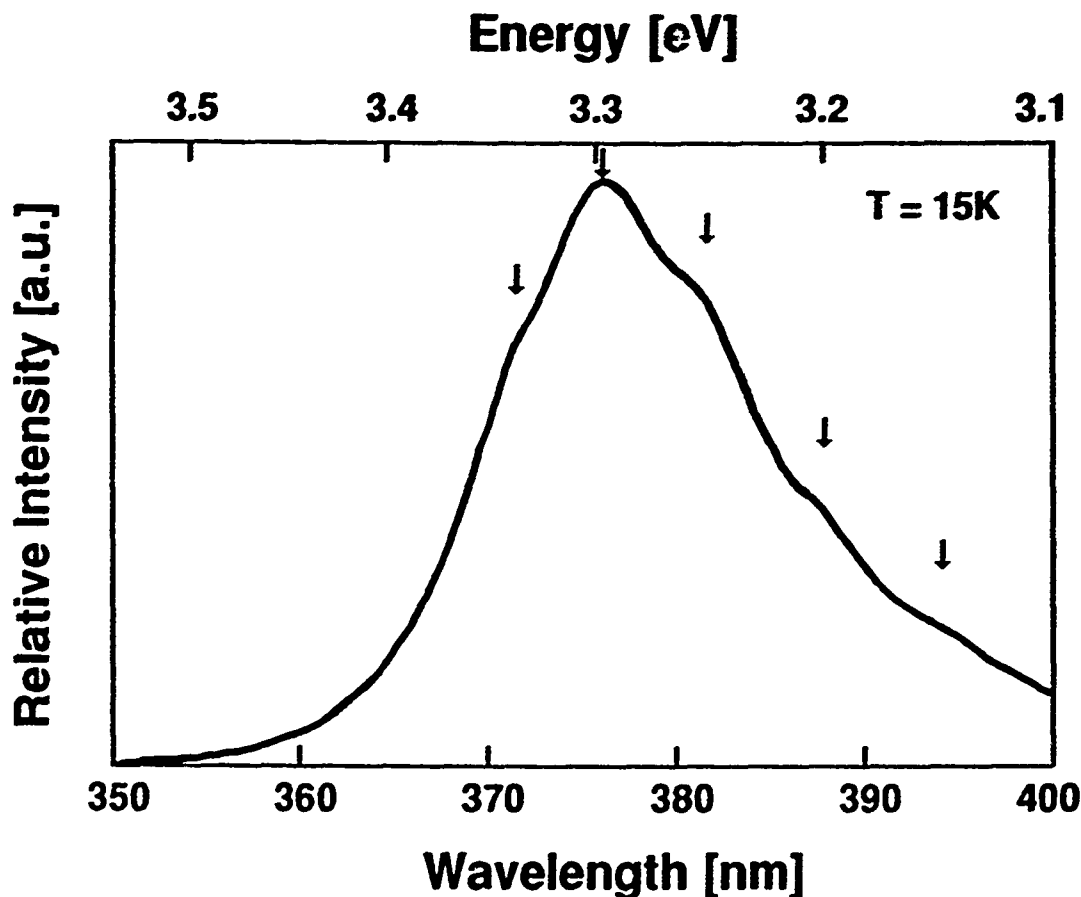

Figure 3.   The edge emission of the cathodoluminescence at 15K from a cGaN epitaxial film. The cluster consists of five, in energy equally-spaced peaks. The spacing is ≈50 meV, and the arrows denote their positions.

D. Summary

The first photo- and cathodoluminescence results obtained from single crystals of the cubic phase GaN have been reported. The bandgap of cGaN was determined to be 3.33 eV at 15K and 3.28 eV at room temperature, which is 140 and 160 meV lower than respective values for the wurtzite phase. The edge emission of cathodoluminescence at 15K showed a cluster of five equally-spaced peaks. This is believed to be caused by phonons with an energy of ≈50 meV. The lattice parameter of 0.451 nm was measured by X-ray diffractometry.

E. References

1. K. Das and D. K. Ferry, Solid-State Electron. **19**, 851 (1976).

2. J. I. Pankove, *Mat. Res. Soc. Proc.* **97**, 409, Materials Research Society 1987.

3. J. I. Pankove, *Mat. Res. Soc. Proc.* **162**, 515, Materials Research Society 1990.

4. W. Seifert and A. Tempel, Phys. Stat. Sol. A **23**, K39 (1974).

5. M. Mizuta, S. Fujieda, Y. Matsumoto, and T. Kawamura, Jap. J. Appl. Phys. **25**, L945 (1986).

6. M. J. Paisley, Z. Sitar, J. B. Posthill, and R. F. Davis, J. Vac. Sci. Technol. A **7**, 701 (1989).

7. T. P. Humphreys, C. A. Sukow, R. J. Nemanich, J. B. Posthill, R. A. Rudder, S. V. Hattangady and R. J. Markunas, *Mat. Res. Soc. Proc.* **162**, 531, Materials Research Society 1990.

8. R. C. Powell, G. A. Tomasch, Y. W. Kim, J. A. Thornton and J. E. Greene, *Mat. Res. Soc. Proc.* **162**, 525, Materials Research Society 1990.

9. H. Morkoc, private communication.

10. J. I. Pankove, J. Luminescence **7**, 114 (1973).

11. J. I. Pankove, and S. Bloom, RCA Rew. **36**, 163 (1975).

12. R. F. Davis, Z. Sitar, and M. J. Paisley, Annual Progress Report, NTIS Ref. No. ADA210380.

23. Z. Sitar, M. J. Paisley, D. K. Smith, and R. F. Davis, Rev. Sci. Instr. **61**, 2407 (1990).

14. See for example: J. I. Pankove, *Optical Processes in Semiconductors*, Dover Publications, Inc., New York (1971).

15. D. D. Manchom, A. S. Barker, P. J. Dean and R. B. Zetterstrom, Solid State

V. The Effect of Electron Beam Irradiation on Mg Doped GaN Thin Films

A. Introduction

Numerous groups have deposited GaN epitaxial thin films [1,2]. However a particular challenge has been the production of p-type material which would allow p-n junctions and GaN-based optoelectronic devices to become a reality. The only devices made to date in this normally n-type material have been metal-insulator-semiconductor (m-i-s) structures, with heavily compensated GaN "i" layer containing up to 10^{22} cm^{-3} of the acceptor dopants of Zn or Mg.

Recently Amano at al. [3,4] observed a dramatic increase of the intensity of the emitted light with time while performing cathodoluminescence measurements on Mg-doped GaN films. Subsequently they found that the resistivity had also increased. Moreover, with sufficiently long electron beam irradiation, the material became p-type and the resistivity decreased. Their films were grown by an organometallic route at 1040°C. The same authors observed similar behavior in Zn-doped GaN thin films [5]. Structural properties remained unchanged after the treatment as was confirmed by x-ray diffraction. However, the mechanisms involved are not yet understood.

The following sections describe the results of similar experiments conducted at NCSU.

B. Experimental Procedure

Magnesium-doped GaN films were deposited on monocrystalline (0001) alpha(6H)-SiC wafers using a modified gas source molecular beam epitaxy (MBE) technique. Effusion cells were used for the evaporation of metallic gallium and magnesium, but a unique, MBE compatible, ECR plasma source [6] was used to activate/dissociate molecular nitrogen prior to deposition. The deposition system as well as the predeposition treatment of the substrates have been described previously [7].

Magnesium-doped GaN films having a thickness ≤ 0.5 μm were deposited in the range of 600-700°C on bare or undoped GaN-coated a-SiC wafers. The undoped layers were about 0.3 μm thick. The doping levels were determined by secondary ion mass spectrometry (SIMS) using a Mg implanted GaN reference standard. The implantation energy and the dose for the standard were 50 keV and 3×10^{15} cm^{-2}, respectively.

Two different arrangements were used for the post-growth electron beam irradiation of the films: 1) a 10 kV RHEED gun, placed in one of the ports normally used for an effusion cell on the MBE, and 2) a scanning electron microscope (SEM). The same electron beam energy of 10 keV, was employed; however, the spot sizes, raster areas and the irradiation times were different from that used with the RHEED gun. Table I shows the parameters for both cases.

Table L The parameters of the electron guns used for the post-growth irradiation.

Electron gun	RHEED	SEM
Electron energy [keV]	10	10
Spot size [dia-μm]	1000	0.2
Electron current [mA]	200	2
Electron current density [mA/cm^2]	2.5×10^4	1.6×10^9
Raster size [cm^2]	4	1
Irradiation time [hrs]	4-15	1-6

Current-voltage (I-V) measurements were conducted before and after selected periods of irradiation using a mercury electrical probe. The diameters of the ohmic and rectifying contacts were five and one mm, respectively. Thermal probe measurements were also performed.

C. Results and Discussion

The low temperature growth produced chemically abrupt junctions between the doped and undoped regions of GaN at all temperatures. Figure 1 shows a SIMS depth profile of a 0.6 μm thick GaN film grown at 600°C. The top 0.45 μm of the film is Mg-doped. Clearly, the diffusion of Mg into the undoped GaN was insignificant during deposition. The Mg atomic concentration levels in the several doped layers were in the range of 10^{20}-10^{21} cm^{-3}.

The resistivity of the doped samples increased significantly (a few orders of magnitude) after electron beam irradiation in the SEM. Several samples became p-type, as confirmed by the I–V and thermal probe measurements. Figure 2 shows the change in the I–V curves obtained from a Mg–doped sample after four consecutive one hour LEEBI treatments. Resistivity clearly increased with the irradiation time, and the process appeared to be additive. The curve asymmetry also changed the exposure time. The n-type material is expected to exhibit a larger absolute current with positive than with the same magnitude of negative bias. The opposite is true for p-type material. An apparent change in the symmetry of the I-V curve was observed for a 0.65 μm thick sample with a Mg concentration of 8×10^{20} cm^{-3}. The I-V curve is shown in Figure 3. The irradiation time was three hours.
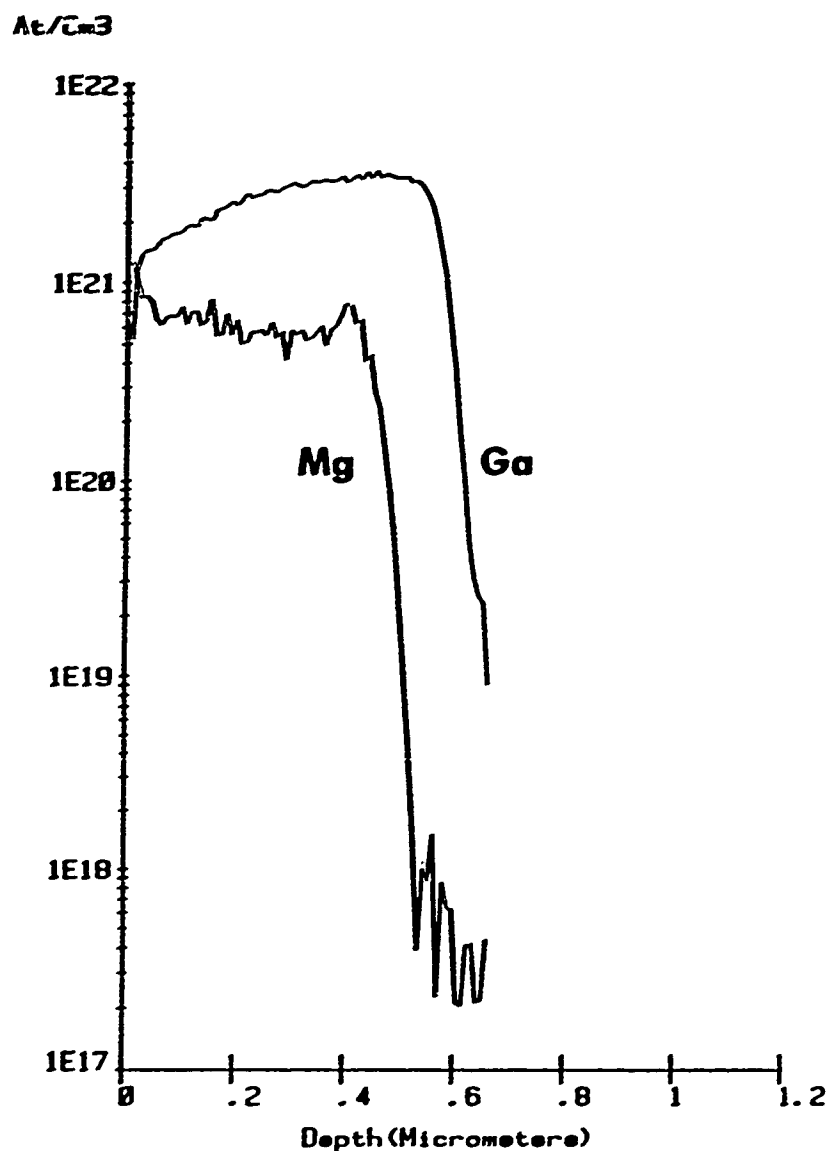
At/Cm3

Figure 1.   SIMS depth profile of an GaN p-n junction. Mg concentration in the p layer
               is ≈6x10²¹ cm⁻³. Note: concentration scale is for Mg only.

A similar procedure performed in the growth chamber using the RHEED electron gun
did not produce any significant changes in the electrical properties of the Mg-doped material
even after 15 hrs of irradiation. Although the electron energy from the RHEED gun was
similar to that used in the SEM, the spot diameter and electron beam current were different.
This difference resulted in almost five orders of magnitude lower electron current density.
Thus the electron current density is an important factor in the activation process of dopants
via LEEBI in GaN. It has no effect unless a threshold current density has been achieved.

Several Mg-doped GaN samples clearly showed p-type conductivity, as confirmed by
I-V and thermal probe measurements. However, a clear dependence of electrical properties
on the irradiation dose was not observed. Moreover, separate irradiation procedures on the
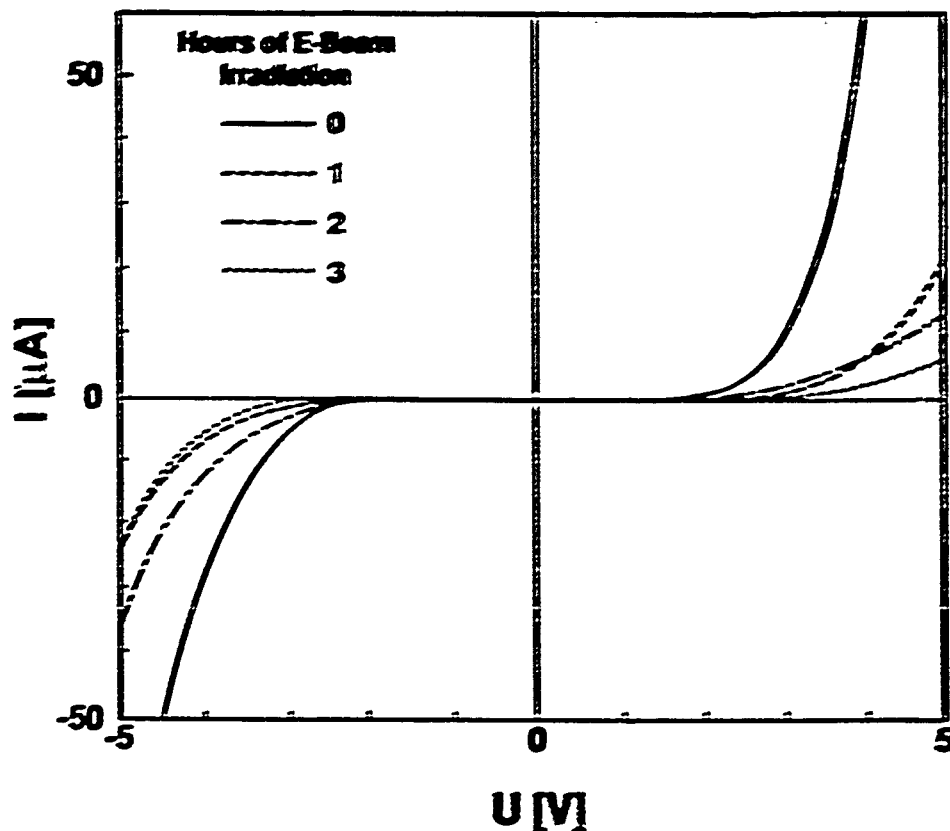
Figure 2. I–V curves of a Mg-doped GaN film before and after three consecutive one hour electron beam irradiations.

different parts of the same wafer did not yield the same changes in the electrical properties. One of the reasons for this inconsistency (maybe the only one) was probably the poor stability of the electron gun used for the irradiation.

Although Amano et al. observed no change in resistivity after the LEEBI treatment of undoped GaN, the resistivity of our undoped samples slightly increased. However the effect was much smaller than with the doped samples.

D. Summary

Monocrystalline Mg-doped GaN thin films have been grown on alpha(6H)-SiC substrates at 600-700°C using modified gas source MBE. SIMS results showed chemically abrupt junctions at all growth temperatures. Samples were post-growth LEEBI treated using a SEM or a RHEED electron gun. Significant changes in the electrical properties including p-type conductivity were observed when the SEM was used, but no changes

were obtained with the RHEED gun. The reason for this is most likely the difference in the electron current densities of the two techniques.
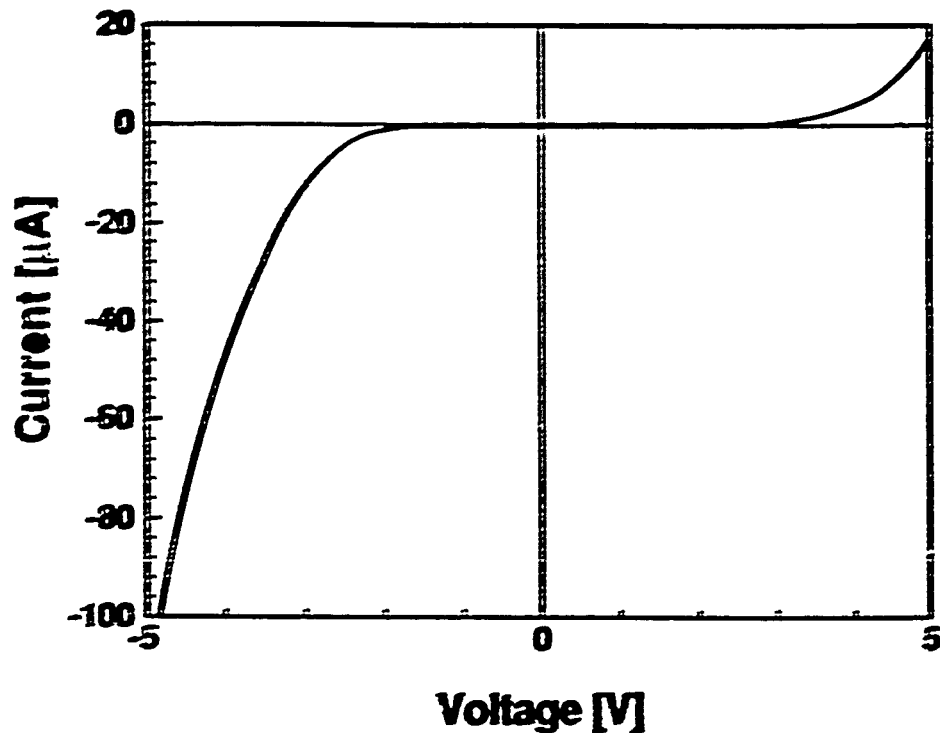
Figure 3.   I-V curve of a Mg-doped and LEEBI treated GaN thin film. The irradiation time and Mg concentration were three hours and $8x10^{20}$ cm^{-3}, respectively.

E. References

1. R. F. Davis, Z. Sitar, B. E. Williams, H. S. Kong, H. J. Kim, J. W. Palmour, J. A. Edmond, J. Ryu, J. T. Glass, and C. H. Carter, Jr., Mat. Sci. & Eng. B 1, 77 (1988).

2. J. I. Pankove, Mat. Res. Soc. Proc. 162, 515, Materials Research Society 1990.

3. H. Amano, M. Kitoh, K. Hiramatsu and I. Akasaki, Proc. 16th Int. Symp. on Gallium Arsenide and Related Compounds, Kanuizawa, Japan (1989).

4. H. Amano, M. Kitoh, K. Hiramatsu and I. Akasaki, Jap. J. Appl. Phys. 28, L2112 (1989).

5. H. Amano, I. Akasaki, T. Kozawa, K. Hiramatsu, N. Sawaki, K. Ikeda and J. Ishii, J. Lumin. 40 & 41, 121 (1988).

6. Z. Sitar, M. J. Paisley, D. K. Smith, and R. F. Davis, Rev. Sci. Instr. 61, 2407 (1990).

7. Z. Sitar, M. J. Paisley, B. Yan, J. Ruan, J. W. Choyke and R. F. Davis, J. Vac. Sci. Technol. B 8, 316 (1990).

VI. GAS-SOURCE MOLECULAR BEAM EPITAXY OF BORON NITRIDE AND GALLIUM NITRIDE

A. Introduction

Boron nitride has long been known for its desirable properties as a highly insulating as well as a chemically and thermally stable material. The cubic phase of boron nitride was first reported by Wentorf,[1] who produced it in a high pressure apparatus. This investigator also conducted the initial measurements regarding the semiconducting properties of this material. It has been used since then primarily for its high hardness in applications such as grinding and polishing. The cubic phase of BN is actually the zinc blende structure or, in space group notation, $\overline{F43m}$ (Hermann-Mauguin) or T_d^2 (Schoenflies). Boron nitride is very similar to carbon in that both exist in hexagonal, wurtzitic, and cubic forms and many of the properties in each of the phases are strikingly similar. For example, both diamond and c-BN are metastable under the conditions currently used for growth of thin films. The primary difference is that hexagonal boron nitride is an insulator and hexagonal carbon is a conductor.

Interest in the cubic polymorph of BN as a semiconductor material has received much interest recently as a possible substrate for the deposition of diamond, due to the similar lattice parameters (Δa_o=1.34%) and its wider bandgap which is in the range of 5.8–6.5 eV.[2–4] Potential applications which would make use of the very wide bandgap of c-BN include optical devices for the vacuum UV (λ~200 nm) and high-power electronic devices. For a complete listing of materials-related properties of c-BN see *Landolt-Börnstein:Numerical Data and Functional Relationships in Science and Technology, Series III, Vols. 17 and 23*, or Ref. [5] (which also includes a side-by-side comparison of properties of c-BN with diamond).

Several approaches have been employed in the attempt to grow thin films of cubic boron nitride (c-BN). These include reactive diode[6] and rf sputtering,[7] ion implantation,[8, 9] plasma CVD,[10–12] microwave plasma CVD,[13, 14] and ion plating techniques.[15–18] These attempts were successful in producing polycrystalline films of c-BN, predominantly of a mixed nature with both cubic and other phases present and of extremely fine grain size. It appears that most researchers succeeded in the deposition of c-BN if the technique included the input of additional energy from energetic ions during the deposition process.

B. Experimental Procedure

The primary deposition technique was GSMBE. Elemental boron and gallium were evaporated from effusion cells, and reactive nitrogen species were obtained by passing molecular nitrogen through a compact electron cyclotron resonance (ECR) plasma source. The growth system was a Perkin-Elmer 430 MBE system modified as described below. It consisted of three major sections: a load lock (base pressure ≈5 × 10⁻⁸ Torr), a transfer tube

(base pressure $=3 \times 10^{-10}$ Torr) which was used to degas the substrates, and the growth chamber (base pressure $=1 \times 10^{-10}$ Torr). The growth chamber was equipped with four standard 20 cc effusion cells and one high-temperature cell, the latter of which contained the B. All metals were contained in BN crucibles which were resistively heated either with Ta or W alloy wire heaters. The gallium cell was loaded with 50 g of 99.999 999% pure gallium.

The special high temperature cell noted above was monitored using a W3%Re-W26%Re thermocouple. Any decomposition of the crucible at the elevated operating temperatures did not affect the growth of the BN films. Prior to installation of the source, the BN crucible was loaded with 3 g of 99.9999% pure boron.

The more significant modification was the use of a compact ECR microwave glow-discharge plasma to dissociate/activate the N-containing gas. This source was designed and commissioned in an in-house effort by Sitar.[19] This source has the advantages of fitting inside the nominal two-inch diameter tube of the source flange cryoshroud and thus minimizes the source-to-substrate distance. As a result, the flux of activated/dissociated species arriving at the substrate surface is increased. This source was attached in place of a more traditional effusion (or cracker) cell for the group V element. The nitrogen gas was taken from a bottle of compressed UHP-grade nitrogen, purified by a metallorganic resin bed gettering material and subsequently regulated to the source by a variable leak valve.

Borazine ($B_3N_3H_6$) contained in a nitrogen carrier gas was also investigated for the deposition of BN, as this chemical is a source for both boron and nitrogen. Borazine was also chosen as a gas source in order to investigate both the activation of this material in the ECR plasma as well as attempt to determine if boron-nitrogen compounds provide a more suitable precursor, since the B–N bond already exists in the material. This was done by placing the borazine (which is liquid at STP) in a temperature controlled bubbler and passing nitrogen gas through it which then passed into the ECR source.

Substrate preparation involved a 30 min. exposure to UV which has been shown to remove hydrocarbon contamination,[20] followed by a dilute acid etch to remove oxide layers. In the case of Si, a solution of H_2O:HF (10:1) was used,[21 and for Cu, a solution of H_2O:HCl (10:1) was employed.[22] Subsequently, the substrates were mounted on a Mo holder using either molten indium or silver paste. Silver paste was very important for the copper substrates as they were extremely sensitive to oxidation and would oxidize heavily in attempting to indium bond the substrates.

Samples were then loaded into a cryopumped load lock. After the initial evacuation, the samples were loaded into the transfer tube where they were degassed to a temperature of 700°C. Immediately after degassing they were loaded into the growth chamber and the deposition cycle initiated. Typical deposition conditions used for both BN and GaN are shown below in Table I.

41

Table I. Deposition Conditions used in GSMBE of BN and GaN

Nitrogen pressure	$1-2\times10^{-4}$ Torr
Microwave power	20–50 W
Boron temperature	1725 – 1775°C
Gallium temperature (where used)	975 – 990°C
UV source power (where used)	500 W
Substrate temperature	400 – 700°C
Growth time (BN)	120 – 360 min.
Deposited film thickness	10–850 Å

The UV lamp, when used, was a 500 W high pressure Hg arc-lamp* with a collimating lens. The resulting spectral output is shown below in Figure 2. Note that the standard units for spectral irradiance are $\mu W\ cm^{-2}\ nm^{-1}$ and thus must be integrated to get power levels. This lamp was setup to illuminate the substrate surface from a sapphire viewport positioned normal to the growth surface. The sapphire window permitted transmission of the entire range of UV wavelengths. Accounting for the mounting geometry and the various losses (including the sapphire window) resulted in an overall illumination power (for the spectrum 200–900 nm) of ~0.5 W cm^{-2}.

---

* Model 6285 lamp in #66042 housing, Oriel Corporation, Stratford, CT 06497
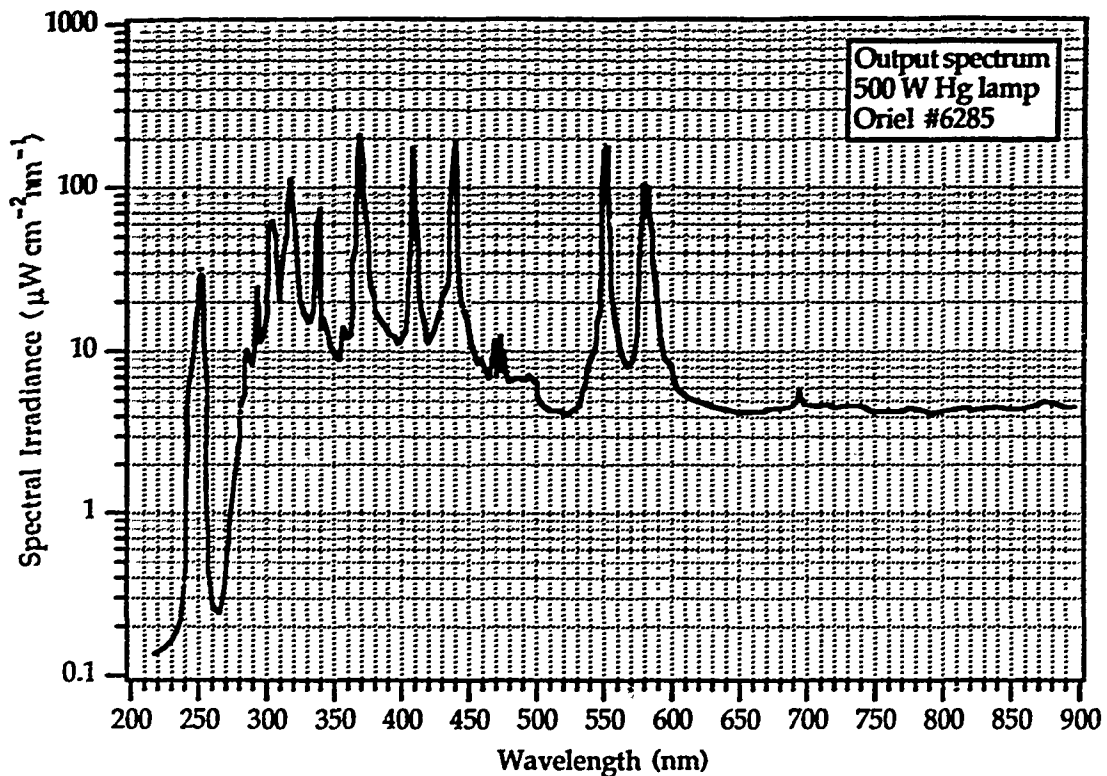
Figure 2. Spectral irradiance plot of the high pressure Hg arc lamp used for photo-enhanced deposition of BN films (After Oriel Corp. data for 500-W Hg-lamp).

Subsequent to deposition, the substrate would either be moved to the load lock for removal from the system or transferred to the analytical system for additional characterization.

C. Results

1. Boron Nitride on Copper. Figure 3 shows an XPS plot (Riber Mac2 analyzer) of BN deposited on a Cu(110) substrate. Note lack of contamination from carbon and oxygen as a result of the UHV deposition. Peak heights make it appear that the surface is primarily Cu. This is not strictly true, since the sensitivity factor for Cu-$2p_{3/2}$ is ~50x greater than that of B-1s and ~10x greater than N-1s. However, significant island formation of BN is strongly suggested.

X-ray spectra (Rigaku Geigerflex) of films grown at two different temperatures are shown in Figure 4. Note that the BN deposit seems oriented to the substrate given that only one reflection is present, but highly defective. This is from the fact that an ordinarily forbidden reflection seems to be present. Deposition does not appear to be affected by the influence of the photon irradiation.

Deposition of BN on Cu (111) was also undertaken to determine effects of substrate orientation. X-ray diffraction showed that the films showed no cubic and were h-BN or t-BN (a planar disordered h-BN variant).
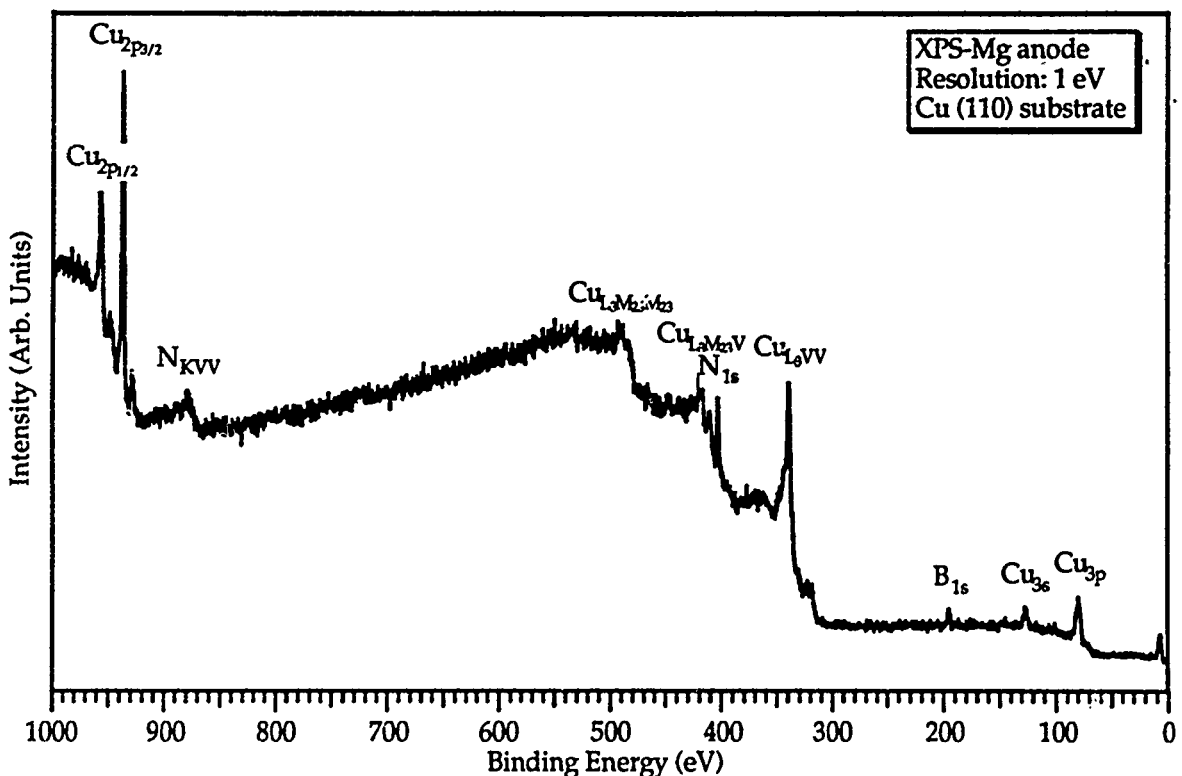
Figure 3.   XPS spectrum of BN deposit on Cu(110) substrate. Cu-$2p_{3/2}$ sensitivity is ~50x greater than that of B-1s and ~10x greater than N-1s.
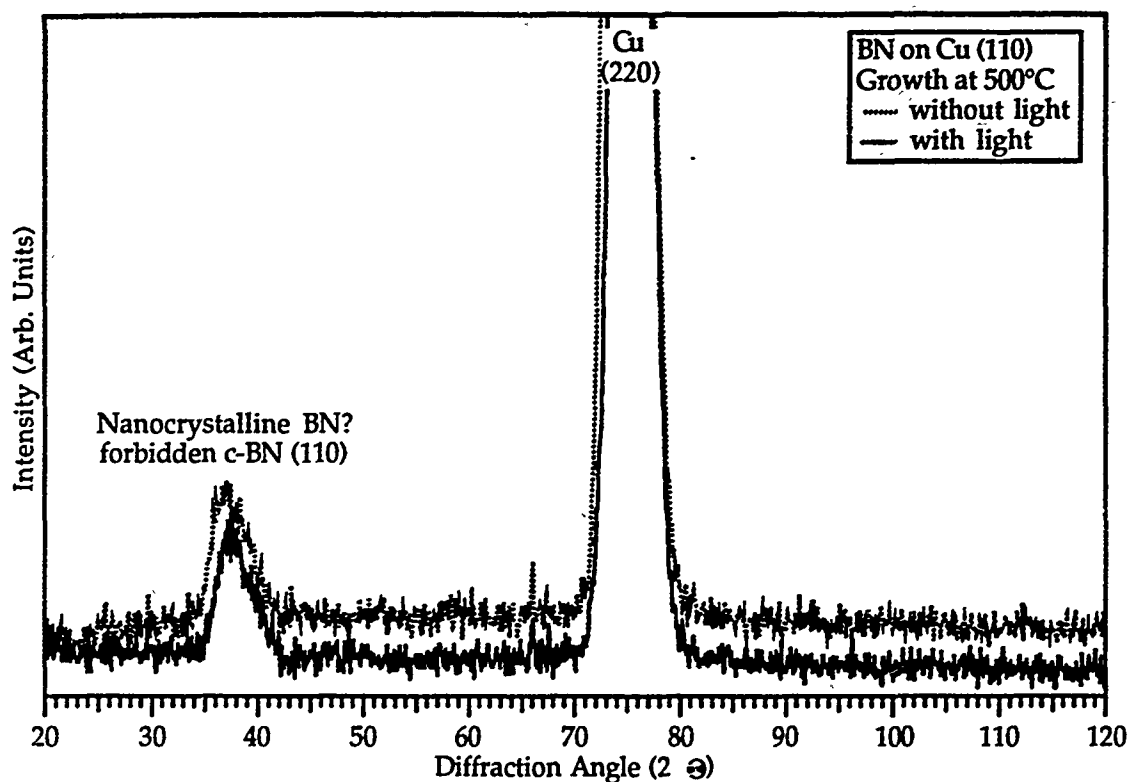
Figure 4.   X-ray spectra (Cu K_α radiation) of BN on Cu (110) substrate.

2. Boron Nitride on Silicon (100). Previous reports from this research program described the FT-IR analysis of films deposited on Si(100). As shown in Figure 5, the films were primarily amorphous; however, they did contain some c-BN component, perhaps in nanocrystalline form.

Subsequent growths attempted to examine the differences that would evolve if the growth surface were illuminated by a high pressure Hg arc lamp. Field emission SEM (Hitachi S-4000) examination results are shown in the following figures. Films deposited without illumination at the higher growth rate are shown in Figures 6 and 7. In the former figure, the film appears free of gross features. However, in Figure 7, an extremely fine texturing on the surface is revealed.

The microstructure of the surface of a film deposited with illumination at the higher growth temperature (500°C) is shown in Figure 8. Since the morphology was essentially the same as Figure 6, a lower magnification micrograph is not shown. Again, the film shows an extremely fine texturing on the surface.
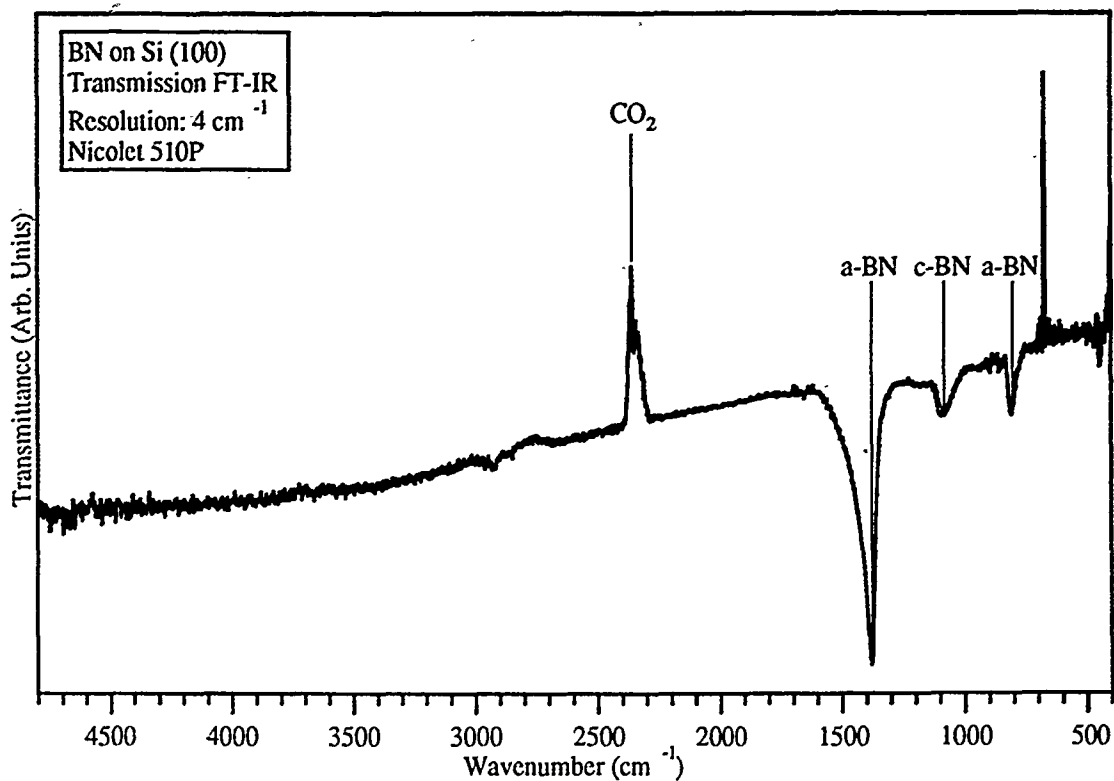
Figure 5. Transmission FT-IR spectra of BN deposited on Si (100) substrate. Inverted CO_2 absorption peak is present because concentration was lower when analyzing sample than for instrument baseline spectrum.
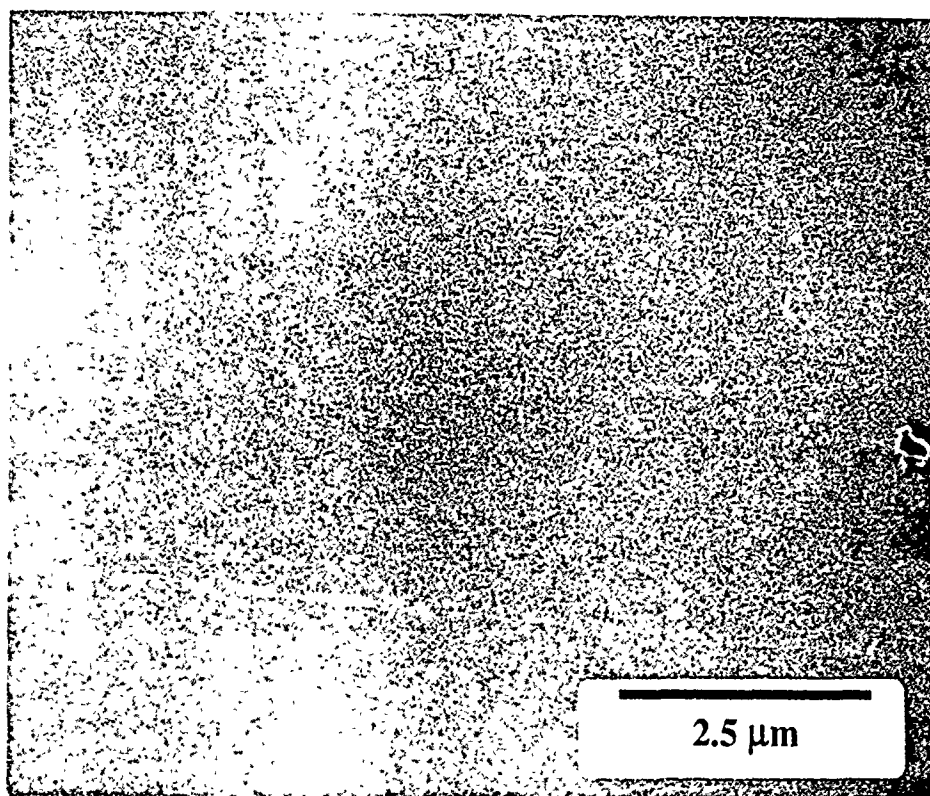
Figure 6. Secondary electron micrograph of surface of BN film deposited on Si (100) without additional illumination (growth at 500°C).
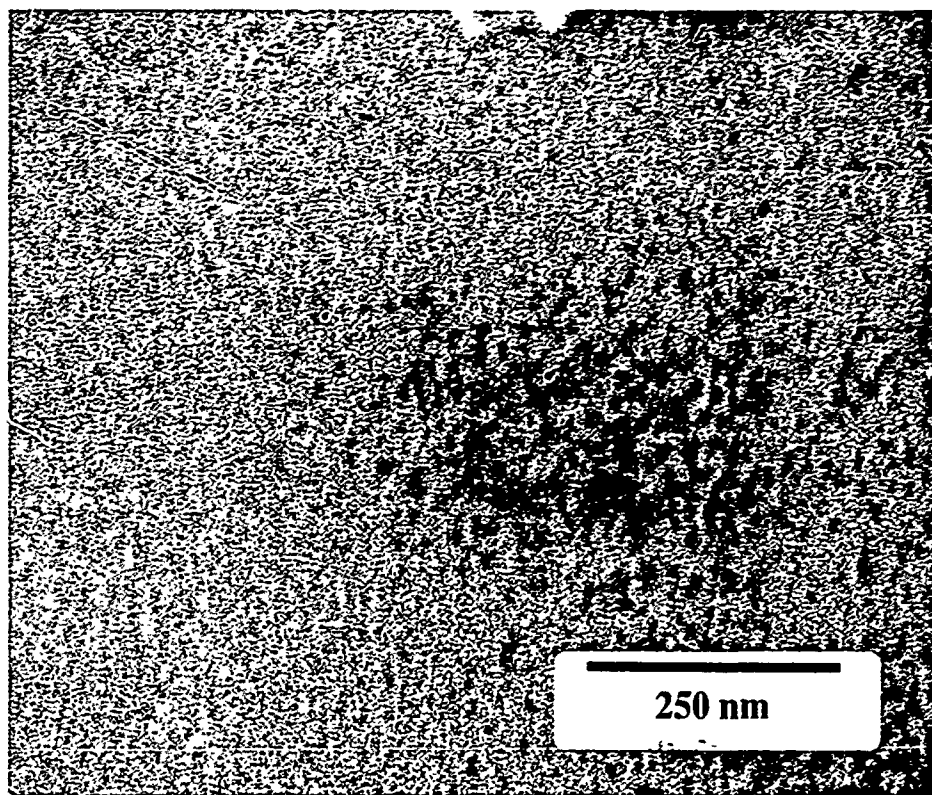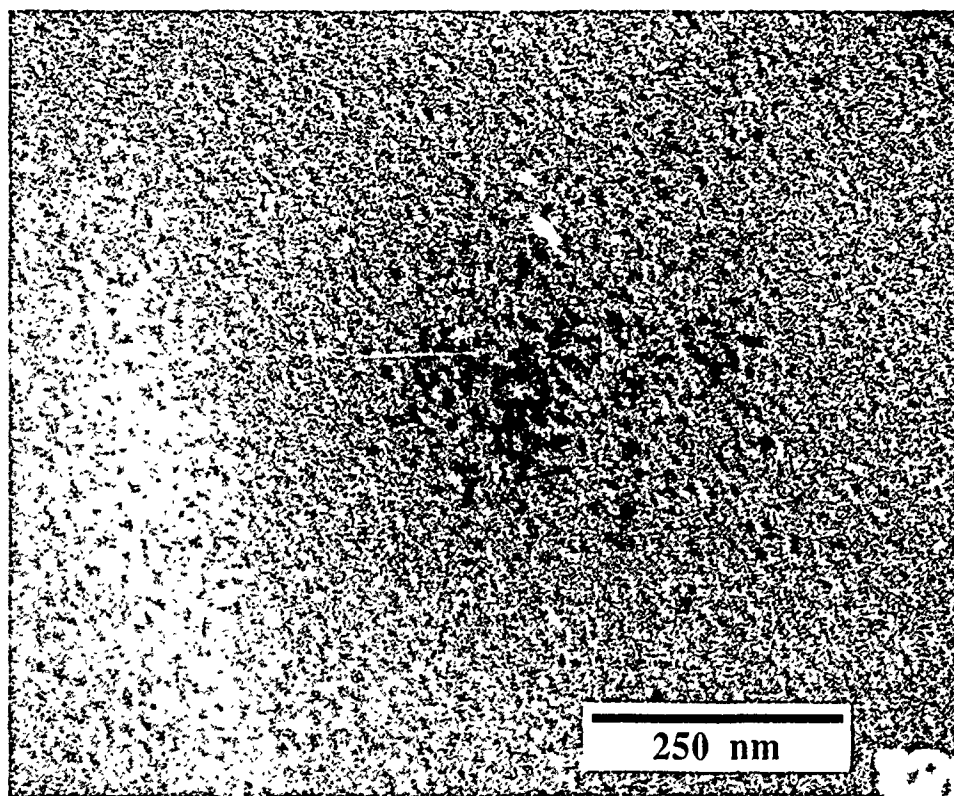
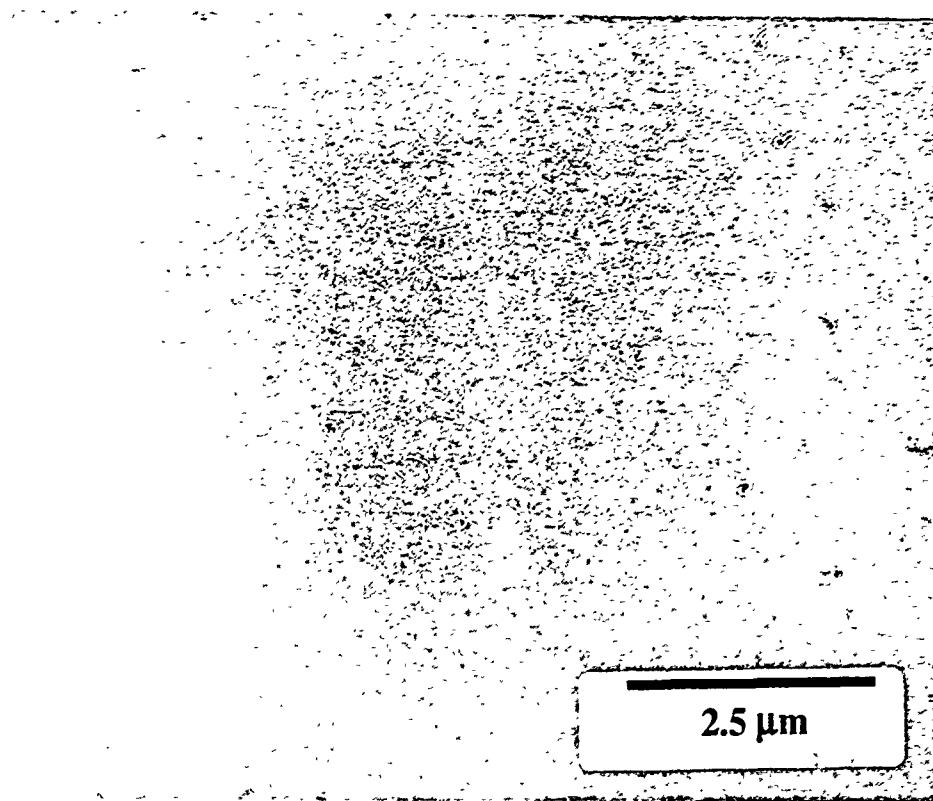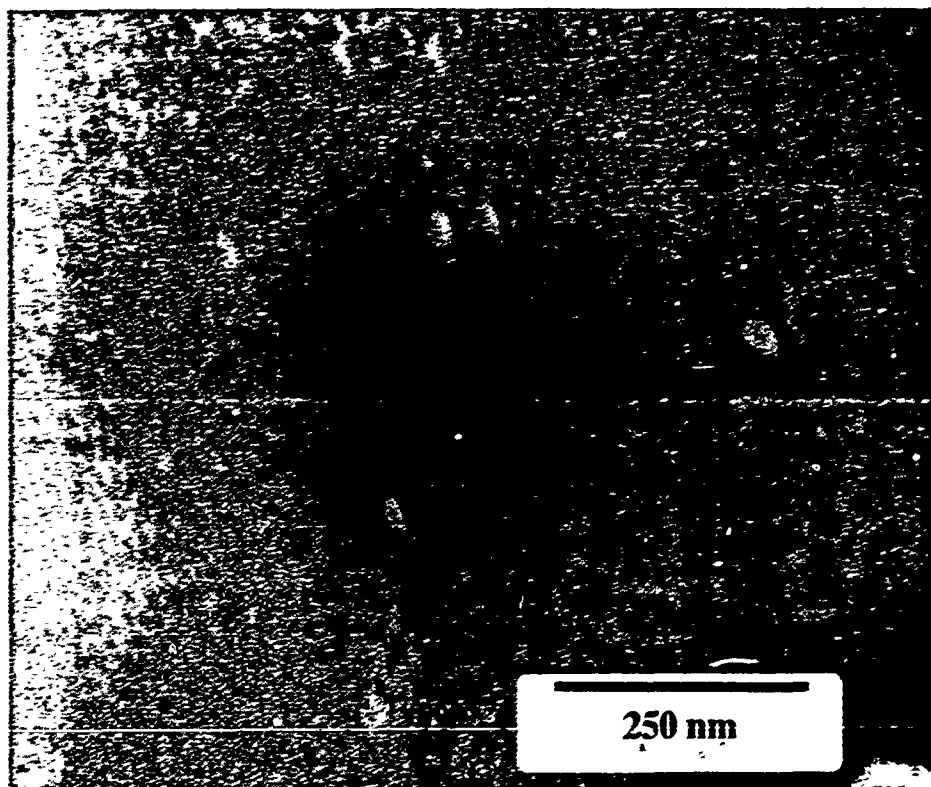Figure 7. Secondary electron micrograph of surface of BN film deposited on Si (100) without additional illumination (growth at 500°C).

Figure 8. Secondary electron micrograph of surface of BN film deposited on Si (100) with additional illumination from the UV source (growth at 500°C).

Growth at a lower temperature (400°C) resulted in the surface morphologies shown in Figures 9 and 10. They reveal a small but discernable change from those shown in Figures 6-8. The higher magnification micrograph of Figure 10 shows small grains across the surface.

Figure 11 shows the surface microstructure for films grown at 400°C in tandem with the illumination from the arc lamp. The microstructure at low magnification was similar to that of Figure 9 and so is not shown. The microstructure is more like that of the films deposited at 500°C, than that of the 400°C film without illumination. However, the change in appearance is slight.

Shown in Figure 12 are the diffraction patterns from depositions at 500°C. Note that the sample with illumination fractured from handling which resulted in a high background at low angles due to the scattering from mounting clay. The interesting feature is that the c-BN (400) peak is not present except when the growth surface is photon irradiated.

Figure 9. Secondary electron micrograph of surface of BN film deposited on Si (100) without additional illumination (growth at 400°C).

48

Figure 10. Secondary electron micrograph of surface of BN film deposited on Si (100) without additional illumination (growth at 400°C).
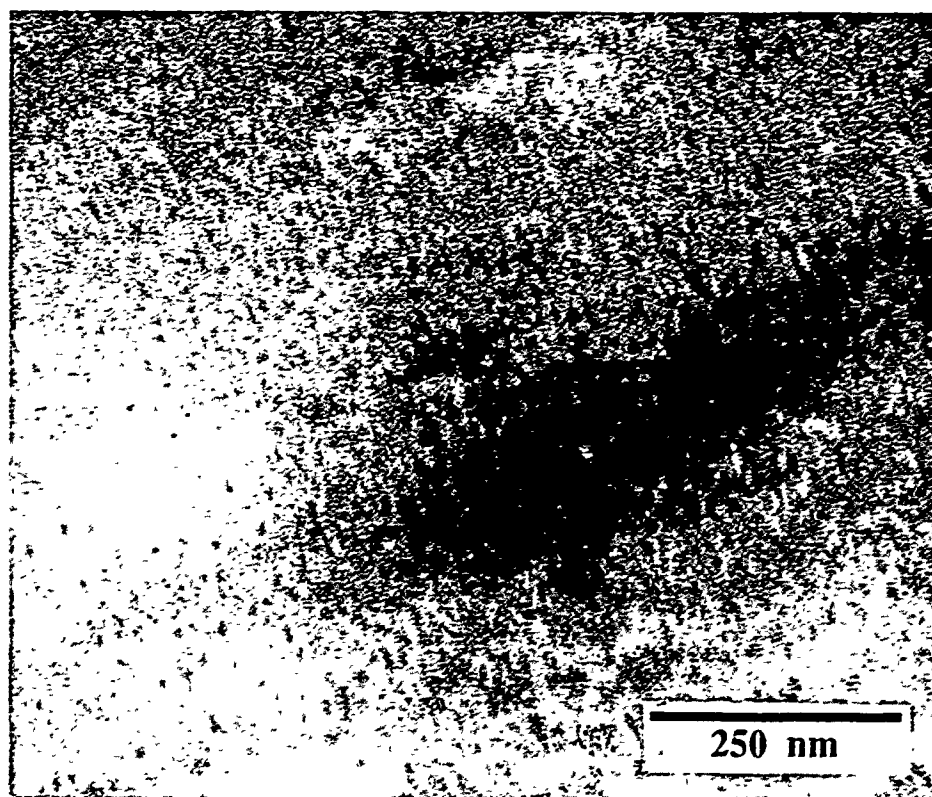

Figure 11. Secondary electron micrograph of surface of BN film deposited on Si (100) with additional illumination (growth at 400°C).
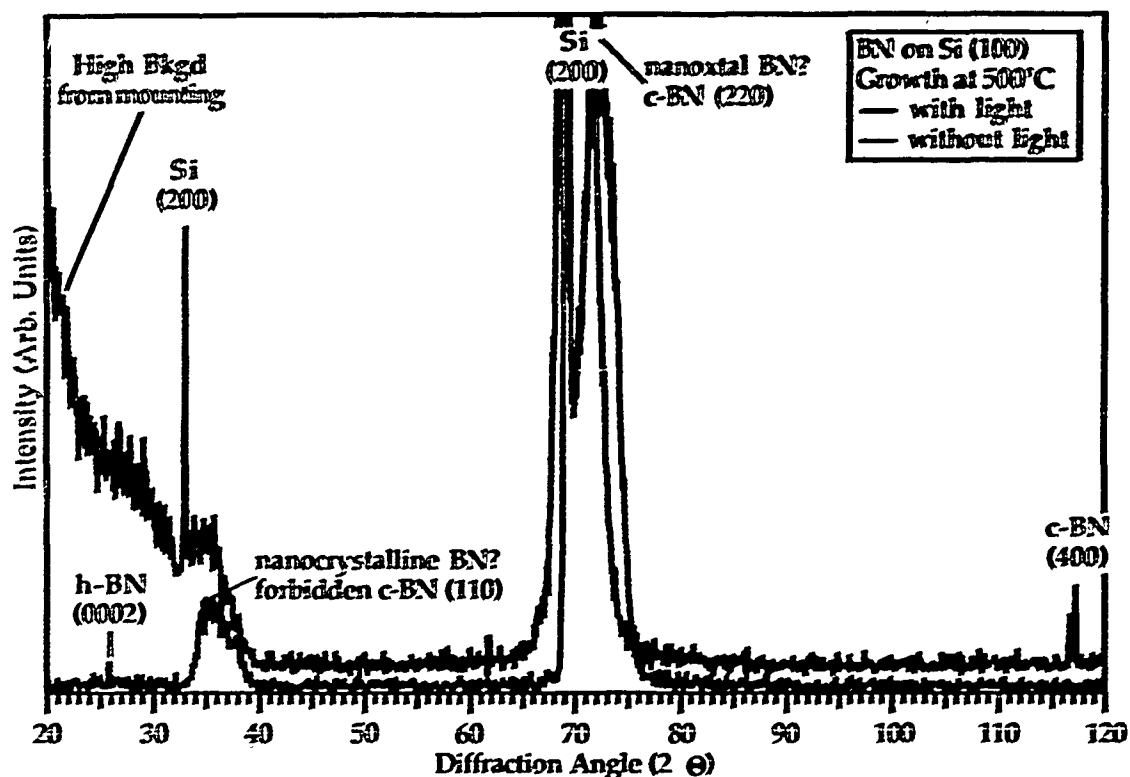
49

Figure 12. X-ray diffraction patterns (Cu K_α radiation) of BN deposited on Si (100) at 500°C with and without illumination from the Hg arc lamp.

Samples were next compared at a lower growth temperature to determine its impact on the phase formation. Figure 13 shows patterns from depositions at 400°C. The h-BN phase is apparently much more well crystallized at this lower temperature, based on the narrow linewidth of the h-BN (0002) peak. In both cases, the c-BN (400) peaks are present, but there is a dramatic decrease in the intensity of the h-BN (0002) peak for the illuminated case, indicating a strong inhibition of the formation of this phase.

The FT-IR spectra from the samples grown at 500°C are shown in Figure 14 and show that there is little else evident than the two phases of BN. Please note that peaks for amorphous BN coincide with those of h-BN and thus are not differentiated in these spectra (see discussion).

The FT-IR spectra for the samples grown at 400°C are shown in Figure 15 and show a much more complex structure. Note the many water and carbon dioxide peaks are from a purging problem in the optical analysis bench and can be ignored. Interestingly, the complex peak structures for the unirradiated case disappeared for the case when the photon irradiation was used. This is not contamination as has been shown in many previous reports from XPS spectra.
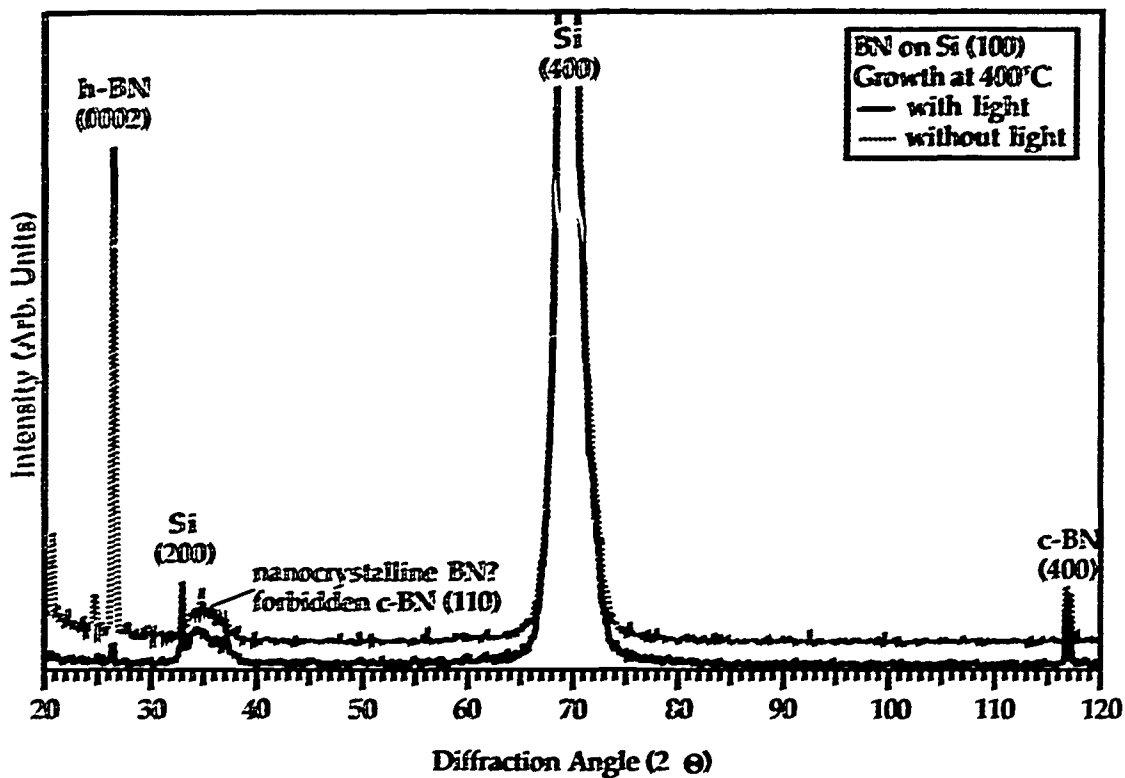
Figure 13. X-ray diffraction patterns (Cu K_α radiation) of BN deposited on Si (100) at 400°C with and without illumination from the Hg arc lamp.
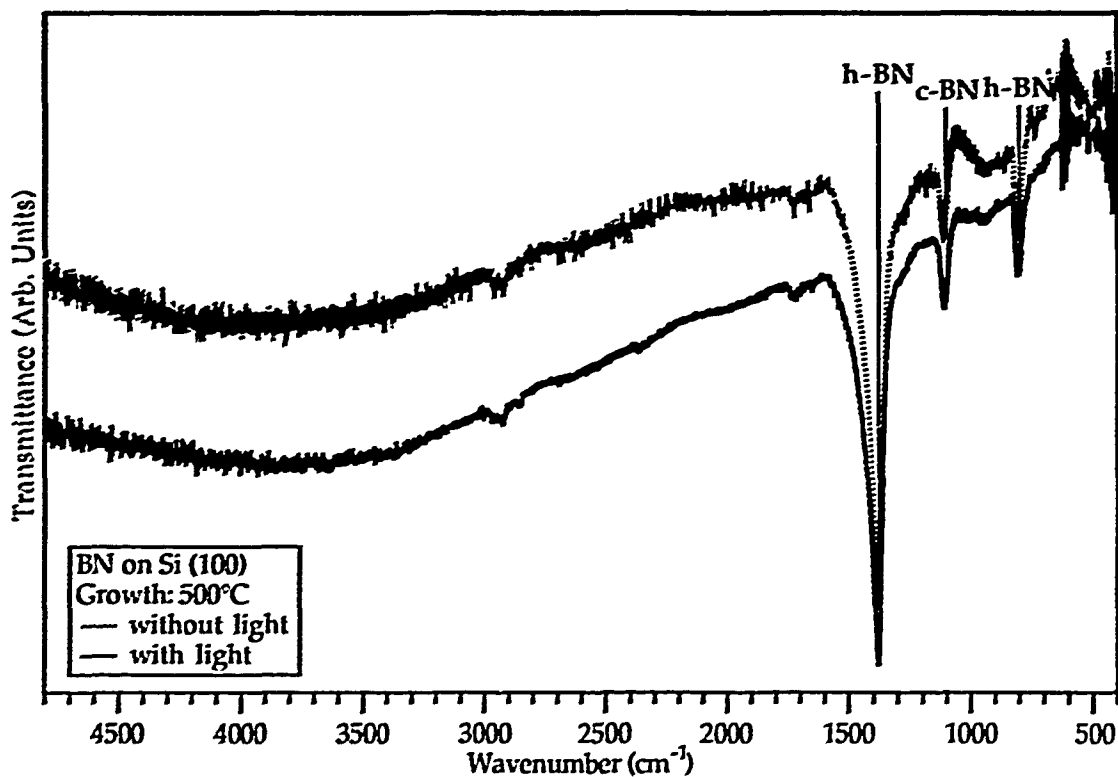

Figure 14. FT-IR spectra (Nicolet 510P) of BN on Si (100) deposited at 500°C.

D. Conclusions

1. Boron Nitride on Copper. Films of a highly defective and microcrystalline c-BN nature were deposited on Cu (110). Films deposited on Cu (111) were clearly different and of a h-BN character, indicating that the substrate had a strong influence on the crystal structure of the BN films.

2. Boron Nitride on Silicon (100). Films deposited without photon irradiation and reported previously were analyzed in this reporting period. These films contained material with cubic character, as revealed by FT-IR studies. Ultra-violet irradiation was shown to have a definite effect on the deposition of the BN films. At 500°C, it enhanced the crystallization of the c-BN phase and did not encourage the formation of h-BN. At 400°C, photon irradiation clearly inhibited the formation of the h-BN phase, which had previously formed more readily at that temperature and did not inhibit the crystallization of the c-BN phase. Illumination of the growth surface also appeared to reduce certain types of cubic-like character in the film, but also removed other types of bonding defects present in the films.

E. References

1. R. H. Wentorf Jr., J. Chem. Phys. 36, 1990 (1962).

2. R. M. Chrenko, Solid State Commun. 14, 511 (1974).

3. C. Deshpandey and R. F. Bunshah, Thin Solid Films 163, 131 (1988).

4. N. Miyata, K. Moriki, and O. Mishima, Phys. Rev. B 40(17), 12028 (1989).

5. R. C. DeVries, Cubic Boron Nitride: Handbook of Properties, Technical Information Series, General Electric Company, Corporate Research and Development, 72CRD178, 1972.

6. K. H. Seidel, K. Reichelt, W. Schaal, and H. Dimigen, Thin Solid Films 151(2), 243 (1987).

7. M. Mieno and T. Yoshida, Jpn. J. Appl. Phys. 29(7), 1175 (1990).

8. M. Satou and F. Fujimoto, Jpn. J. Appl. Phys. 22(3), L171 (1983).

9. Y. Andoh, et al., Nucl. Instrum. Meth. Phys. Res. B19/20, 787 (1987).

10. J. Kouvetakis, V. V. Patel, C. W. Miller, and D. B. Beach, J. Vac. Sci. Technol. A 8(6), 3929 (1990).

11. H. Saitoh, T. Hirose, H. Matsui, Y. Hirotsu, and Y. Ichinose, Surf. Coat. Technol. 39–40(1–3), 265 (1989).

12. M. Okamoto, H. Yokoyama, and Y. Osaka, Jpn. J. Appl. Phys. 29(5), 930 (1990).

13. A. Chayahara, H. Yokoyama, T. Imura, and Y. Osaka, Appl. Surf. Sci. 33/34, 561 (1988).

14. O. Matsumoto, M. Sasaki, H. Suzuki, H. Seshimo, and H. Uyama, in *Tenth International Conference on Chemical Vapor Deposition*, G. W. Cullen, Eds. (The Electrochemical Society, Honolulu, Hawaii, 1987), pp. 552.

15. T. Hada, Y. Kawate, and Y. Hirai, Kobelco Technol. Rev. **6**, 1 (1989).

16. M. Murakawa and S. Watanabe, Surf. Coatings Technol. **43/44**(1-3), 128 (1990).

17. E. Nagatomo, Y. Hirooka, and O. Omori, Trans. IECE Jpn. E **69**(4), 432 (1986).

18. T. Hada, Y. Kawate, and Y. Hirai, J. Vac. Sci. Technol. A **8**(4), 3168 (1990).

19. Z. Sitar, M. J. Paisley, D. K. Smith, and R. F. Davis, Rev. Sci. Instrum. **61**(9), 2407 (1990).

20. J. R. Wig, J. Vac. Sci. Technol. A **3**(5), 1027 (1985).

21. H. Lamb, private communication, 1990.

22. I. Villegas, C. B. Ehlers, and J. L. Stickney, J. Electrochem. Soc. **137**(10), 3143 (1990).

INDEX OF TECHNICAL REPORTS

INDEX OF ALL PUBLICATIONS

A. Papers Published in Refereed Journals

1. R. F. Davis. Z. Sitar, B. E. Williams, H. S. Kong, H. J. Kim, J. W. Palmour, J. A. Edmond, J. Ryu, J. T. Glass and C. H. Carter, Jr., "Critical Evaluation of the Status and the Areas for Future Research Regarding the Wide Band Gap Semiconductors of Diamond, Gallium Nitride and Silicon Carbide," Journal of Materials Science and Engineering B: Solid State Materials for Advanced Technology, Vol. B., 77–104.

2. M. J. Paisley, V. Sitar, J. B. Posthill and R. F. Davis, "Growth of Cubic Phase GaN by Modified Molecular Beam Epitaxy," Journ. Vac. Sc. Technol. A 7, 701-5 (1989).

3. R.F. Davis, "High Temperature Semiconducting Materials and Devices," Physics Today 43, 57 (1990).

4. M.J. Paisley, Z. Sitar, Benda Yan and R.F. Davis, "Growth of Boron Nitride Films by Gas Source Molecular Beam Epitaxy," Jour. Vac. Science and Technol. A **8**, 32 (1990).

5. Z. Sitar, M. J. Paisley, B. Yan, J. Ruan, J. W. Choyke and R. F. Davis, "Growth of AlN/GaN Layered Structures by Gas Source Molecular Beam Epitaxy," J. Vac. Sci. Technol. B **8**, 316 (1990).

6. Z. Sitar, M. J. Paisley, D. K. Smith and R. F. Davis, "Design and Performance of an Electron Cyclotron Resonance Plasma Source for Standard Molecular Beam Epitaxy Equipment," Rev. Sci Instrum. **61**, 2407 (1990).

7. Z. Sitar, M. J. Paisley, B. Yan, J. Ruan, J. W. Choyke and R. F. Davis, "AlN–GaN Superlattices Grown by Gas Source Molecular Beam Epitaxy," Thin Solid Films **200**, 311 (1991).

8. M.J. Paisley, Z. Sitar, Benda Yan and R.F. Davis, "Growth of Films by Gas Source Molecular Beam Epitaxy," Jour. Vac. Science and Technol. A **8**, 323 (1990).

9. R. F. Davis, "Large Bandgap Electronic Materials and Devices," *Proceed. IEEE*, **79**, 1 (1991).

10. R. F. Davis, "III - V Nitrides for Electronic and Optoelectronic Applications," *Proceed. IEEE* **79**, 702 (1991).

11. Z. Sitar, M. J. Paisley, J. Ruan, J. W. Choyke and R. F. Davis, "Luminescence and Lattice Parameter of Cubic Gallium Nitride," J. of Mat. Sci. Lett., **12**, 88 (1992).

B. Books (and sections thereof) Published

1. R.F. Davis, "Research on Various Electronic Thin Films in Japan," *Department of Defense Scientific Information Bulletin,* **15** [3] 48 (1990).

2. "Large Bandgap Electronic Materials and Components," Special Issue of the Proceedings of the IEEE, ed. by R. F. Davis, The Institute of Electrical and Electronics Engineer, Inc., New York, NY, 1991.

3. Z. Sitar, M. J. Paisley, B. Yan and R. F. Davis, "Structural Defects in GaN Epilayers Grown by Gas Source Molecular Beam Epitaxy," in *Diamond, Silicon Carbide and Related Wide Bandgap Semiconductors,* Materials Research Soc. Symp. Proceed. 162, J. T. Glass, R. F. Messier and N. Fujimori, eds., Materials Research Society, Pittsburgh, PA, 1990, pp. 537-541.

4. R.F. Davis, "Current Status of the Research on III-V Mononitride Thin Films for Electronic and Optoelectronic Applications," in *The Physics and Chemistry of Carbides, Nitrides and Borides,* R. Freer, ed. Kluwer Academic Publishers, Dordrecht, The Netherlands, 1990, pp. 653 - 669.